FROM LINEAR TO BOTTLEBRUSH: MATERIAL PROPERTY CORRELATIONS OF ACRYLATE ELASTOMERS

Benjamin Jared Morgan

A dissertation submitted to the faculty at the University of North Carolina at Chapel Hill in partial fulfillment of the requirements for the degree of Doctor of Philosophy in the Department of Chemistry.

Chapel Hill
2021

Approved by:

Sergei Sheiko

Wei You

Scott Warren

Theo Dingemans

Stephen Craig

ABSTRACT

Benjamin Jared Morgan: From Linear to Bottlebrush: Material Property Correlations of Acrylate
Elastomers
(Under the direction of Sergei Sheiko)

This dissertation aims to advance the current understanding of graft polymer architectures

and the new and unique properties that can be accessed by their application to elastomeric materials.

Current accessible polymer materials are synthesized from linear polymer architectures, which

have been implemented to great effect and restructured the economy and technology of the world.

However, in the case of linear elastomers the only architectural control parameter that can be tuned

is the crosslink density, n_x, which imposes a fundamental limitation on the accessible material

properties limiting their modulus ($G > 100\ kPa$), maximum extensibility ($\lambda_{max} < 5$), and strain-

stiffening characteristics ($\beta < 0.20$). Here we have studied graft polymer elastomers made from

poly(butyl acrylate) (PBA) to draw correlations between their architectural parameters (sidechain

length-n_{sc}, grafting density-n_g, backbone length-n_{bb}, and crosslink density-n_x) and their material

properties. A series of loosely grafted comb polymers in the melt were examined by oscillatory

shear rheology to study how the entanglement modulus of such architectures can be tuned by

varying the n_{sc}, and n_g. A model system created from PBA graft polymer elastomers was

introduced and used to correlate the mechanical and swelling properties of graft polymer

elastomers with their associated architectural parameters. Of particular note it was found that graft

polymer architectures could provide a unique opportunity to develop tissue like gels, whose

mechanical properties can be tuned independently of their solvent fraction. Lastly, the electroactive

properties of bottlebrush elastomers were shown to be large strains at low operating voltages.

To my family and friends.

ACKNOWLEDGMENTS

I would like to acknowledge my advisor Sergei Sheiko for his generous support at the beginning of my scientific career. He has provided me with a great opportunity to advance my understanding of the world around me and gave me space when I needed to grow. You have become a transformation character in my life who shaped who I am as a scientist and a person.

The lab I stumbled in happen to have a collection of wonderful colleague I was able to learn from. Special thanks are given to Daixuan Zhang, Yidan Cong, Matthew Everhart, Will Daniel, Andrew Keith, Qiaoxi Li, and Xiaobo Hu. No journey is worth the effort if you can't surround yourself with wonderful people along the way.

I must also acknowledge the efforts of all the collaborators who help make all the work in this thesis possible. Thank you Daniel Armstrong, Heyi Liang, Guojun Xie, Andrey Dobrynin, Krzysztof Matyjaszewski, and Alfred Kleinhammes. You are all scientists of great distinction and wouldn't have gotten this far without your generous efforts.

TABLE OF CONTENTS

LIST OF TABLES

LIST OF FIGURES

LIST OF ABBREVIATIONS

ATRP   Atom transfer radical polymerization

BAPO   (2,4,6-trimethylbenzoyl)-phosphine oxide

CHAPTER I

BIOMIMETIC TECHNOLOGY

1.1 Introduction

Nature is a constant source of inspiration for science and has led to the development of many new materials that are soft, biocompatible, and designed to function as biological implants or integrate existing technologies into the human body.[1-2] One striking difference between traditionally engineered polymeric materials compared to their biological counterparts is their observed difference in material properties. In general, traditional materials are rigid whereas biological materials are soft and elastic.[3] In particular, the commonly synthesized polymeric elastomers tend to be crosslinked from linear polymer strands and their materials properties are a result of their specific chemical identity and the number of crosslinks per unit volume. This inherently limits them to both a narrow range of material properties. Biological materials on the other hand show a diverse range of material properties even from chemically identical materials.

The sharpest contrast between biological elastic materials and their synthetic counterparts is observed in the materials modulus and extensibility. Biological materials tend be soft, low modulus, and firm or highly strain stiffening. However, many synthetic materials elastomers do not directly mimic this behavior. At high crosslink densities, linear elastomers are hard and rigid, whereas at low crosslink densities the materials are semi-soft and elastic.[4] In fact, the lower limit of a linear elastomers modulus is often higher than many biological elastic materials. Since a lowering in the materials chemical crosslink density causes no change to the materials entanglement density, which

1

is a property of the specific chemicals being used. Ultimately, at the lowest crosslink densities physical entanglements dictate the mechanical properties and consequently make it impossible to replicate biological tissues.

The sharpest contrast between biological elastic materials and their synthetic counterparts is observed in the materials modulus and extensibility. Biological materials tend be soft, low modulus, and firm or highly strain stiffening. However, many synthetic materials elastomers do not directly mimic this behavior. At high crosslink densities, linear elastomers are hard and rigid, whereas at low crosslink densities the materials are semi-soft and elastic.[4] In fact, the lower limit of a linear elastomers modulus is often higher than many biological elastic materials. Since a lowering in the materials chemical crosslink density causes no change to the materials entanglement density, which is a property of the specific chemicals being used. Ultimately, at the lowest crosslink densities physical entanglements dictate the mechanical properties and consequently make it impossible to replicate biological tissues.

The most common solution to resolve the difference in material properties between synthetic elastomers and biological materials is to swell a linear network in a solvent. This results in a decrease in the materials modulus and also make the material more strain stiffening. Both of these characteristic are a result of stretching out the linear strands so that they are pre-extended, while also decreasing the number of mechanically active strands for each unit volume of the material. The consequence of following this strategy is often premature device failure due to leakage of the solvent upon material deformation or evaporation. Implants especially are known to cause many adverse side effects when they leach solvent and plasticizer into the human body. However, even with these side effects gels are the predominant material which is used to make synthetic biological materials.

This work intends to follow a different route by using more complex bottlebrush and comb architectures to lower an elastomers modulus, while increasing the materials strain stiffening behavior. The materials mechanical properties, physical structure, and swelling characteristics have been studied. These materials have been shown to be a promising strategy to mimicking the mechanical properties of biological tissues and this work will further investigate its effectiveness.[5]

1.2 Bottlebrush and Comb Elastomers

Bottlebrush and comb elastomers are a more complex polymer architecture than traditional linear elastomers and will be refered to in this text as graft polymers, combs, or bottlebrushes. Similar to linear elastomers they have a crosslink density connecting load bearing strands that give them their elastic properties. However, they also contain grafted sidechains and this additional control parameter is the defining characteristic that gives them their unique properties. **Figure 1.1** shows the main architectural control parameters that are used to characterize this subset of polymer architectures.
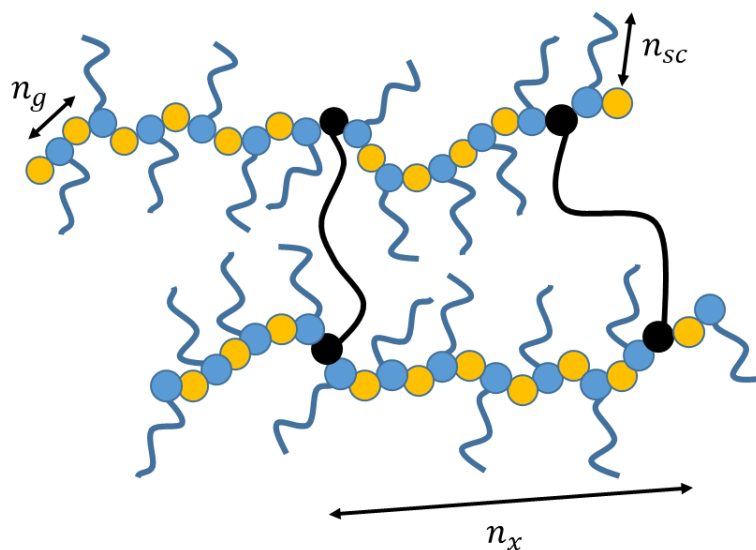
Figure 1.1: Graft polymer architectural parameters. Graft polymer architectures are characterized by three primary control parameters, [n_{sc}, n_g, n_x]. The sidechain length, n_{sc},

corresponds to the number of monomeric units on the backbone of the grafted sidechain. The grafting density, n_g, is the average number of monomeric units between grafted sidechains. The crosslink density, n_x, is the number of backbone units between crosslinks. Each circle along the back bone corresponds to one monomeric unit, where the blue circles attach to a grafted sidechain and the yellow circles are spacers between sidechains. The black circles correspond to crosslinks between different backbones.

The sidechain length, grafting density, and crosslink density refer to the three control parameters used to characterize branched polymer networks. The sidechain length, n_{sc}, referes to the degree of polymerization of the polymers grafted sidechains. The grafting density, n_g, is the number of number of monomeric units between grafted sidechains counting the backbone units the sidechains are grafted to. The crosslink density, n_x, is the same as linear networks and is the number of backbone units between crosslinks.

For the remainder of this thesis, the nomenclature [n_{sc}, n_g, n_x] will be used to refer to specific polymer architectures and [n_{sc}, n_g] will be used to refer to a series of graft polymers that each have a differing crosslink density. An example, in **Figure 1.1** the polymer would be described as [10,2,13] assuming that the degree of polymerization of the grafted sidechains is 10 monomeric units in length. If there are a series of samples that all have a sidechain length of 10 ($n_{sc} = 10$) monomeric units and an average grafting density of 2 ($n_g = 2$) then those samples will be referred to as the [10,2] series.

1.3 Synthesis of Graft Polymer Architectures

Graft polymer architectures are more complex than linear polymers and multiple different strategies have been used to create similar architectures.[6-7] The main strategies are "grafting through", "grafting to", and "grafting from" (**Figure 1.2**).[8]

4
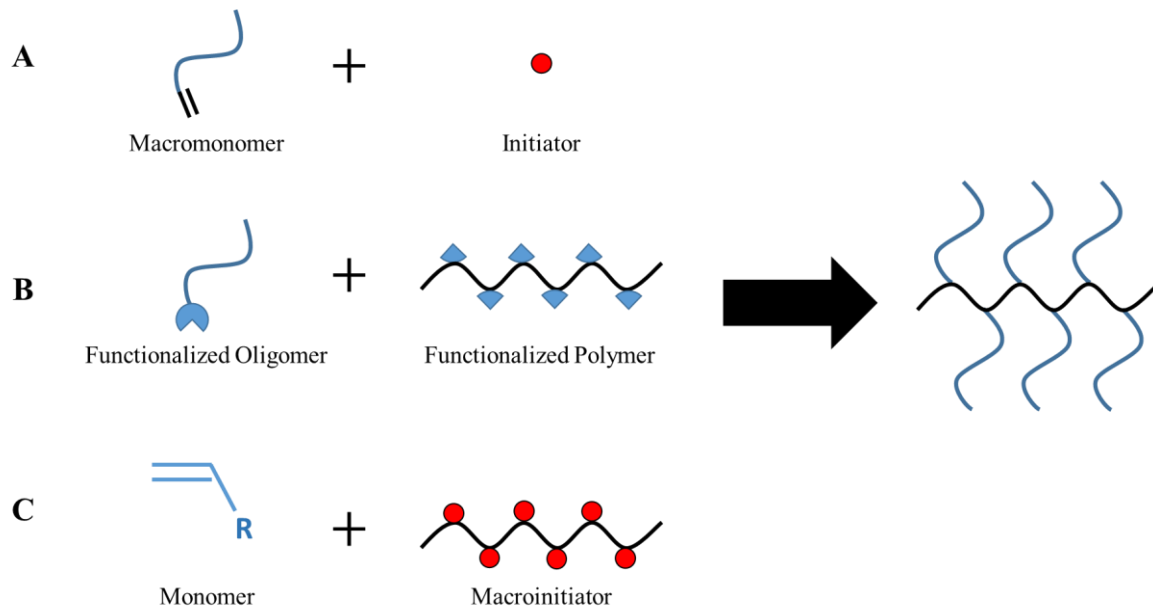
Figure 1.2: Synthesis of graft polymer architectures. Graft polymers can be synthesized three different ways. (**A**) They can be "grafted through" from macromonomers. (**B**) They can be "grafted to" a functionalized polymer. (**C**) The sidechains can be "grafted from" a macroinitiator.

Grafting through refers to the polymerization from macromoners containg polymerizable end groups. This strategy is the simplest way to synthesize bottlebrush and comb elastomers, but it can be difficult to produce melts with long backbones due to the steric hindrance from bulky macromonomers and inherently lower monomer concentraions used during synthesis. Grafting to implies that pendant sidechain groups are attached to a pre-formed polymer backbone and this approach can also be used to synthesize elastomer to great effect, but requires that the backbone and sidechains be soluble with eachother or a cosolvent. Grafting from is where sidechinas are polymerized off of a larger polymer backbone and is primarily used to sythesize long polymer melts, often, with a sparser grafting densities than what is achievable by the other two methods. In this work, the grafting through approach has been used to synthesize bottlebrush and comb

elastomers using a free radical controlled polymerization using macromonomers. The grafting

from approach has also been used to synthesize melts of graft polymers containing large backbones.

1.4 Atom Transfer Radical Polymerization

This work leverages the use of ATRP towards the development of acrylate macromonomers to

synthesize polymer brushes using a grafting through approach. To this end it is important to have

a basic understanding what ATRP is and how it is conducted. The mechanism for ATRP is show

in **Figure 1.3**.

$$P_nX \quad + \quad M_t^m(L)_z \quad \underset{k_{da}}{\overset{k_a}{\rightleftharpoons}} \quad P_n^\bullet \quad + \quad XM_t^{m+1}(L)_z$$

$$k_p \qquad k_t$$
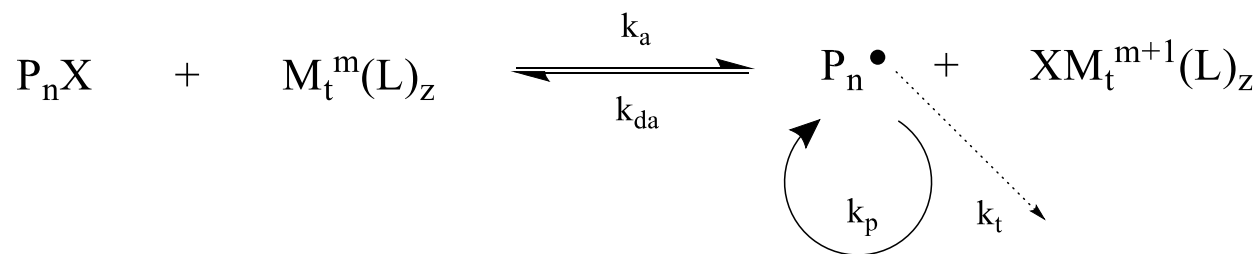
Figure 1.3: Atom transfer radical polymerization mechanism. The mechanism for ATRP is
one such that the propagating chain (P_n) is either in its active ($P_n\bullet$) or deactivated (P_nX) state, which
is mediated by a metal ligand complex ($M_t^m(L)_z$) that undergoes reversible chain transfer with a
halide atom. The reactivity of the complex is such that $k_a \ll k_{da}$ which causes very few instances of
chain propagation at any one time. Since termination is only possible during the short window of
time during chain propagation these events are rare.

 ATRP is a controlled radical polymerization. This means that under normal operating conditions

radical termination at the progpoaging chain end is rare and it is possible to polymerize well define

polymers with a narrow molecular weight distribution. This is accomplished through the use of a

metal ligand complex which allows the polymerizing chain end to undergo chain transfer with a

halogen atom. The reaction rate between activation and deactivation of the propogating chain end

is such that it heavily favors the deactived state, so that when propogation is switched on there is

small chance that propoagation will occur and a a monomer will be added to the propogating chain

before it is placed once again in its deactivated state. This type of reversible chain transfer controls the rate of chain propogation minimizing the amount of chain termination events, while also controlling the length of the propogating chains in solution. Also, a halogen atom will be present at the end of the chain after polymerization is terminate, which allows for a simple post polymerization modification to be made to generate macromonomer.

There are several different styles of ATRP that one can use. The type used in this work is called supplemental activator and reducing agent (SARA) ATRP, which uses Cu^0 as a supplemental activator and a reducing agent that can regenerate the catalyst after it undergoes oxidation. This is particularly useful because it decreases the oxygen sensitivity of the reaction and qualitiativley improves the process of conducting the polymerization. From a practical approach this is a method that can be recommended for making functional polymeric materials in a laboratory setting and has been used in this work to make batch sizes ranging between 100-500 g for each polymerization.

1.5 Outline

This work will focus on the development of graft polymer architectures to study the relationship between a polymers architecture and its material properties. Oscillatory shear rheology will be used to study a series of PBA comb polymers to investigate how their entanglement length changes with respect to the architectural parameters n_{sc}, n_g, and n_{bb} which refer to the sidechain length, grafting density and length of the polymer backbone (**Chapter 2**). Then this understanding will be applied to the development of PBA graft polymer elastomers, for which a model system will be synthesized where the entire graft polymer elastomer is made from simple acrylate monomers (**Chapter 3**). The mechanical properties of these elastomers will be studied by using their stress strain curves to extract the material parameters G and β, which can

then be used to describe the correlation between the elastomers architecture and its material properties (**Chapter 4**). The swelling behavior of these elastomers will then be investigate because they can be used as a unique materials design platform toward the development of tissue like elastomers, which can, at the same solvent fraction, display a large range of mechanical properties (**Chapter 5**). This thesis will conclude with the application of bottlebrush architectures towards dielectric elastomer actuators for which they have been shown to generate high actuation strains at low applied electric fields (**Chapter 6**).

REFERENCES

1. Kim, Byung-Soo, and David J. Mooney. "Development of biocompatible synthetic extracellular matrices for tissue engineering." *Trends in biotechnology* 16, no. 5 (1998): 224-230.

2. Lee, Kuen Yong, and David J. Mooney. "Hydrogels for tissue engineering." *Chemical reviews* 101, no. 7 (2001): 1869-1880.

3. Ilievski, Filip, Aaron D. Mazzeo, Robert F. Shepherd, Xin Chen, and George M. Whitesides. "Soft robotics for chemists." *Angewandte Chemie* 123, no. 8 (2011): 19301935.

4. Vatankhah-Varnosfaderani, Mohammad, William FM Daniel, Matthew H. Everhart, Ashish A. Pandya, Heyi Liang, Krzysztof Matyjaszewski, Andrey V. Dobrynin, and Sergei S. Sheiko. "Mimicking biological stress–strain behaviour with synthetic elastomers." *Nature* 549, no. 7673 (2017): 497-501.

5. Daniel, William FM, Joanna Burdyńska, Mohammad Vatankhah-Varnoosfaderani, Krzysztof Matyjaszewski, Jarosław Paturej, Michael Rubinstein, Andrey V. Dobrynin, and Sergei S. Sheiko. "Solvent-free, supersoft and superelastic bottlebrush melts and networks." *Nature materials* 15, no. 2 (2016): 183-189.

6. Verduzco, Rafael, Xianyu Li, Stacy L. Pesek, and Gila E. Stein. "Structure, function, selfassembly, and applications of bottlebrush copolymers." *Chemical Society Reviews* 44, no. 8 (2015): 2405-2420.

7. Feng, Chun, Yongjun Li, Dong Yang, Jianhua Hu, Xiaohuan Zhang, and Xiaoyu Huang. "Well-defined graft copolymers: from controlled synthesis to multipurpose applications." *Chemical Society Reviews* 40, no. 3 (2011): 1282-1295.

8. Lee, Hyung-il, et al. "Stimuli-responsive molecular brushes." *Progress in polymer science* 35.1-2 (2010): 24-44.

CHAPTER II

RHEOLOGICAL PROPERTIES OF ELASTOMERS AND MELTS

2.1 Introduction

Compared to linear polymers the larger number of control parameters available for graft polymer networks and melts makes them the most logical choice for improving the material properties of traditionally linear materials. In fact, the entanglement of linear polymer chains fundamentally limits the modulus of a polymer melts ($>10^5$ Pa) and the extensibility simple of rubbers ($\lambda<5$). Especially, the larger degree of control available over the entanglement modulus from fine tuning the molecular architecture parameters n_{sc}, n_g, and n_{bb} provides unprecedented advantage to that of linear polymer.[1-3] If you can control the entanglement modulus of polymer melts you can also control related properties of elastomer materials including extensibility, firmness, strain stiffening, and the strength of the material.[4-7] Ultimately, by leveraging the unique aspects of this material it is possible to advance the state of the art in many applications involving soft polymer materials.

Fetters *et. al.* has provided two simple expressions for poly(α-olefins) that estimate the plateau modulus $G_N{}^0$ simply from its chemical structure using the parameter m_b, the average molecular weight per backbone bond.

$$G_N{}^0 = 24,820 m_b{}^{-3.49} \ (m_b = 14 - 28) \tag{2.1}$$

$$G_N{}^0 = 41.84 m_b{}^{-1.58} \ (m_b = 35 - 56) \tag{2.2}$$

These expressions have been used in the literature to qualitatively examine bottlebrush and comb polymers.[8-9] However, little evidence has been gathered to explain the physics behind this simple empirical relationship. Herein we expand upon previously published theory on bottlebrush and comb polymer melts[1] to clarify the simple empirical model presented above.

Previously[1] defined separate conformational regimes to describe the transition from linear to bottlebrush polymers. Starting at low grafting density the loosely-grafted comb regime (LC) is characterized by branching side chains, whose degree of polymerization (n_{sc}) is less than the degree of polymerization of the polymer backbone between side chains (n_g). In this regime both the backbone and side chains are in random Gaussian conformations and the side chains are physically separated in space. Side chains are surrounded by neighboring molecules and not neighboring side chains. When the degree of polymerization of the backbone becomes similar to the degree of polymerization of the side chain ($n_g = n_{sc}$) the conformation of the polymer transitions into the densely-grafted comb regime (DC). Here, the pervaded volume of side chains on the same molecule start to overlap. As n_g decreases further side chains interact less with the side chains or neighboring molecules and share more of their pervaded volume with side chains from the same backbone. At the onset of the loosely-grafted brush regime (LB), n_g has decreased to the point where neighboring side chains become fully separated from the side chains of neighboring molecules ($n_g = n_g^*$). Decreasing n_g further results in the extension of the polymer backbone, which is later followed by extension of the polymer sidechains. The denselygrafted brush regime (DB) begins when the polymer backbone is nearly fully extended and further decrease in the grafting density stretches the polymer sidechains increasing the distance between neighboring backbones.

This study can be found butyl acrylate combs have been synthesized using a grafting with varying grafting densities, and at high molecular weights. The simple empirical model from equations **5.1** and **5.2** have been vastly improved upon and reflect the behavior of materials over a wide range of grafting densities. More detail can be found in the official publication of this work and has been briefly summarized here.

2.2 Theory

The theory summarized here can be found in more detail in the cited published paper.[9] Graft polymers differ greatly to those of linear polymers due to their increased number of architectural parameters with which they can be described. For graft polymer architectures an accurate way of characterizing their behavior can be done be describing them using what will be defined as the compositional parameter φ and the crowding parameter Φ. The compositional parameter corresponds to the volume fraction of backbone monomer in graft polymer and can be simply described the architectural parameters n_{sc} and n_g.

$$\varphi = \frac{n_g}{n_g + n_{sc}} \qquad 2.3$$

The crowding parameter however has much less of a physical meaning for bottlebrush architectures and can be simply used to understand classify under which architectural parameters a particular regime of behavior a material is likely to fall into. The physical description used for the crowding parameter is the volume fraction of monomers a specific graft polymers monomers, V_m, within the same graft polymers pervaded volume of its sidechains, V_p.

$$\Phi = \frac{V_m}{V_p} \qquad 2.3$$

Assuming that the sidechains are operating as ideal chains ($R_{sc} = (bln_{sc})^{1/2}$) and adding this to our understanding that the composition parameter is simply the volume fraction of backbone monomer in the graft polymer the relationship can be described as,

$$\Phi \cong \frac{v}{(bl)^{3/2}} \varphi^{-1} n_{sc}^{-1/2}$$

2.3

where v, l and b are the corresponding monomer projection length, Kuhn length and monomer volume for the specific monomer the graft polymer sidechains. Using this parameter as to classify graft polymers with their architectural parameters, the comb regime, the stretched backbone (SBB) regime, and the stretched sidechain (SCC) regime are characterized by $\Phi < 1$, $\Phi \approx 1$, and $\Phi > 1$. The specific regime boundaries are given in **Table 2.1.**

Table 2.1: Regime boundaries and corresponding effective Kuhn length.

Regime		Regime boundaries[a]	Kuhn length, b_K
Comb		$\varphi^{-1} \leq (bl)^{3/2} n_{sc}^{1/2}$, for $n_{sc} l > b$ $\varphi^{-1} \leq l^3 v^{-1} n_{sc}^2$, for $n_{sc} l < b$	b
Bottlebrush	SBB	$(bl)^{3/2} n_{sc}^{1/2} \leq \varphi^{-1} \leq bl^2 v^{-1} n_{sc}$	$bl^{-3/2} b^{-1/2} \varphi^{-1} n_{sc}^{-1/2}$
	SSC	$bl^2 v^{-1} n_{sc} \leq \varphi^{-1} \leq l^3 v^{-1} n_{sc}^2$	$v^{1/2} l^{-1/2} \varphi^{-1/2}$

[a] l - bond length, b - Kuhn length of the linear polymer strand, and v - monomer volume.

2.3 Rheology of Combs

A series of six comb samples were received from the Matyjaszewski group and were synthesized using a grafting through approach. ATRP copolymerization of nBA and HEA-TMS was used to from the backbone of the backbone of the comb samples. Then backbones were deprotected and functionalized with α-bromoisobutyryl bromide to form a macroinitiator. The macroinitiator was

then used to initiate the polymerization of nBA to grow the corresponding sidechains along the polymer backbone. The reaction scheme can be seen in **Figure 2.1**.

$$n_g = \frac{n_{b1}}{n_{b2}} + 1$$

$$n_{bb} = n_{b1} + n_{b2}$$
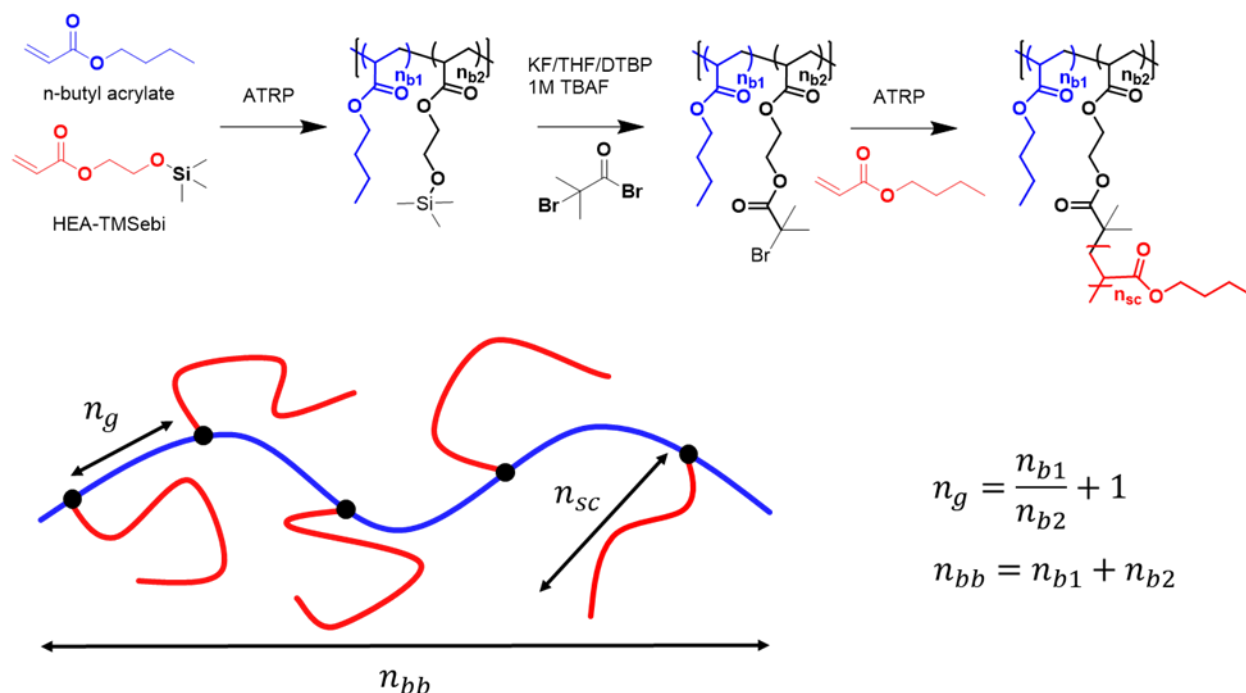
Figure 2.1: Synthesis of butyl acrylate combs. Reaction scheme for combs synthesized by the Matyjaszewski group at Carnegie Melon University. Poly(n-butyl acrylate) sidechains spacers showing that the degree of polymerization of the backbone, n_{bb}, is the summation of the PBA spacer, n_{b1}, and sidechains, n_{b2}. The grafting density, n_g, is related to the molar fraction of spacer added during synthesis, where $n_g = n_{b1}/n_{b2} + 1$.

Oscillatory shear rheology was used to measure the entanglement modulus of each polymer. Master curves were produced using time-temperature superposition and all master curves were generated at a reference temperature of 25 °C. **Figure 2.2a** shows polymers $n_g = 3$ and $n_g = 5$, which were synthesized with *n*-butyl methacrylate backbones. **Figure 2.2b** shows the polymers with larger n_g, which were all synthesized with butyl acrylate. For the $n_g = 3$ and $n_g = 5$ polymers, the methacrylate backbone accounts for ~5% and ~8% of the polymers total mass fraction and

the polymers mechanical properties including entanglement modulus should not deviate much from those with a completely acrylate backbone.
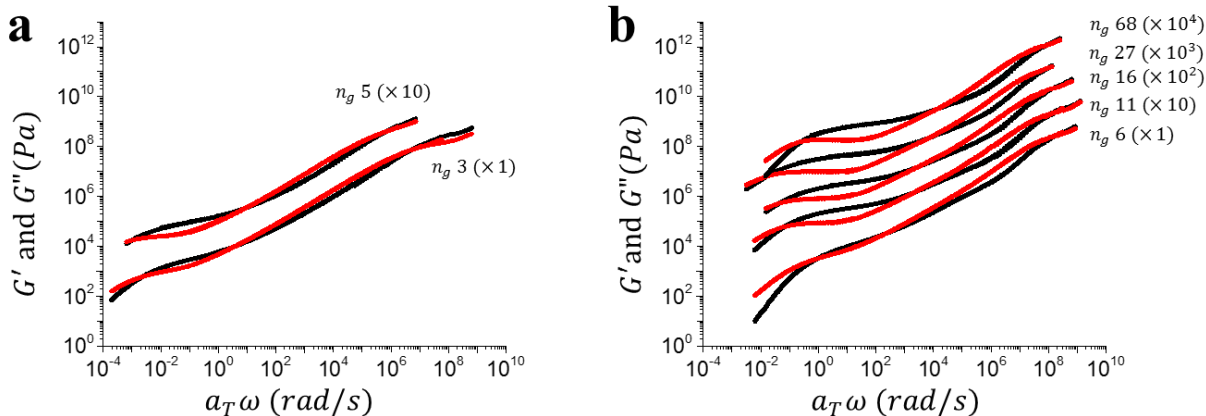
Figure 2.2: Rheological Mastercurves of PBA combs. Dynamic Master curves of the sorage modulus G' (black lines) and loss modulus G'' (red lines) were measured for the graft polymers with (a) poly(butyl methacrylate) and (b) poly(butyl acrylate) spacers between sidechains. The frequencies given are for 25 C, where the α_T is the frequency shift factor at a reference temperature of 70 C. The curves are vertically shifted by an indicated factor between 10 and 10^4 Pa so that they can be easily distinguished from one another.

The entanglement plateau of the bottlebrush and comb polymers can be seen in **Figure 2.2**. For the polymers with methacrylate backbones (**Figure 2.2a**) the plateau is between 10^{-3} and 1 rad/s and the acrylate backbone polymers (**Figure 2.2b**) the entanglement plateau is seen between 10^{-1} and 100 rad/s. The curves have been offset from each other by a factor between 10 and 10^3. The sample with $n_g = 6$ shows only a slight plateau and this is because n_{bb} was barely long enough to show a slight crossover of the storage modulus over the loss modulus. A polymer with $n_g < 6$ could not be prepared with an acrylate backbone and shows the necessity for using the acrylate backbone at higher grafting densities. The plateau modulus was measured as the storage modulus at the minimum of $\tan(\delta)$ as a function of the $G'(\square)$ in this range (**Table 2.2**).

15

Table 2.2: Structural parameters of synthesized elastomers

$n_g{}^a$	$n_{sc}{}^b$	$n_{bb}{}^c$	$M_{n,theory}{}^d$	$M_{n,GPC}{}^e$	Đ^e	G_e $(kPa)^f$
68	14	2100	359000	300000	1.22	75.5
27	13	2600	535000	476000	1.38	44.4
16	15	2700	690000	474000	1.31	32.0
11	13	3300	910000	520000	1.26	31.2
6	15	3000	1400000	420000	1.57	9.8
5*	13	5000	2420000	972000	1.14	8.1
3*	14	5700	4430000	1210000	1.24	2.7

^{a}Calculated based on the monomer to initiator ratio and conversion determined by ^1H NMR in copolymerization of HEA-TMS (or *HEMA-TMS) and *n*-BA (or *n*-BMA). ^{b}Calculated based on ratio of peaks by ^1H NMR spectrum of backbones. ^{c}Calculated based on monomer to initiator ratio and conversion determined by ^1H NMR in polymerization of *n*-butyl acrylate. ^{d}Calculated based on molecular parameters. ^{e}Determined by SEC using linear polystyrene standards. ^{f}Calculated as the storage modulus at the minimum of $\tan(\delta)$.

Figure 2.3a shows the PBA combs plotted onto the diagram of states for PBA graft polymer architectures. The synthesized combs clearly fall in to the comb regime with the exception the comb with the smallest grafting density. This point falls onto of the transition region from combs to bottlebrushes. It is difficult get true coverage of the bottlebrush regime due to fact that the sidechains need to be long while also having a high grafting density, $n_g \sim 1$. This is incredibly difficult to synthesize synthetically, which is why the green data points have been added from another publications.[1] However, even though these grafting densities are higher ($n_g \sim 1.5$) and the sidechains are longer there is still much room for improvement in terms of coverage of the SSC regime. The SBB regime has also not been covered by the measured sample and represents an opportunity for further studies of the entanglement modulus of PBA melts in the future. In fact, these samples would represent a viable intermediate challenge to tackle first compared to covering more of the SSC regime due to the less stringent synthetic requirements necessary to produce those specific samples. The dotted lines on **Figure 2.3a** represent the crossover point between the combs with flexible sidechains and combs with rigid sidechains. In large the rigidity of these sidechains

comes in part from the fact that they are very short and have considerably fewer conformations that they can adopt compared to longer sidechains.
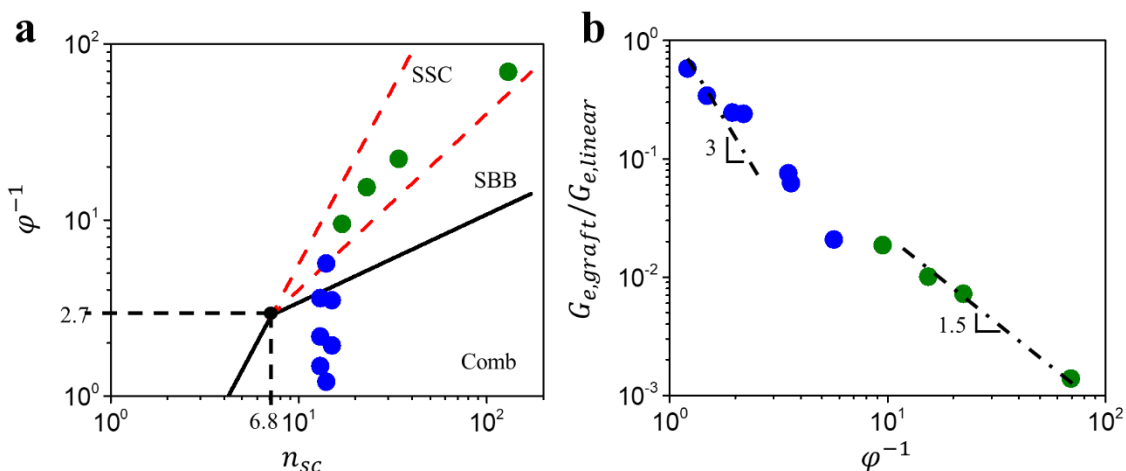
Figure 2.3 Diagram of states for graft polymer architectures. (**a**) Diagram of states showing PBA combs (blue) and bottlebrushes[1] (green). The solid black line represents the regime boundary for the crossover point between the comb and SBB regime. The red dashed lines represent the regime the regime boundary for the crossover point between the SBB regimes into the SCC regime. All crossovers are multiplied by a correction factor of 0.7 which was determined in computer simulations.[10] (**b**) The normalized entanglement modulus plotted against the compositional parameter. PBA combs are shown in blue and bottlebrushes are shown in green.

The normalized entanglement modulus is shown in **Figure 2.3b**. When plotted against the compositional parameter the combs should have a slope of -3 and the bottlebrush samples should have a slip of -3/2. However, it is clear that all of the comb samples do not quite match up with the dashed line drawn in the figure. This is because as the samples move towards the comb regime the go through a broad transition zone between combs and bottlebrush elastomers. In fact, if you look at the combs with the highest compositional parameter then you will notice that they are indeed closest to matching a slope of -3.

REFERENCES

1.   Daniel, William FM, Joanna Burdyńska, Mohammad Vatankhah-Varnoosfaderani, Krzysztof Matyjaszewski, Jarosław Paturej, Michael Rubinstein, Andrey V. Dobrynin, and Sergei S. Sheiko. "Solvent-free, supersoft and superelastic bottlebrush melts and networks." *Nature materials* 15, no. 2 (2016): 183-189.

2.   Fetters, Lewis J., David J. Lohse, César A. García-Franco, Patrick Brant, and Dieter Richter. "Prediction of melt state poly (α-olefin) rheological properties: the unsuspected role of the average molecular weight per backbone bond." *Macromolecules* 35, no. 27 (2002): 10096-10101.

3.   Abbasi, Mahdi, Lorenz Faust, Kamran Riazi, and Manfred Wilhelm. "Linear and extensional rheology of model branched polystyrenes: From loosely grafted combs to bottlebrushes." *Macromolecules* 50, no. 15 (2017): 5964-5977.

4.   Keith, Andrew N., Charles Clair, Abdelaziz Lallam, Egor A. Bersenev, Dimitri A. Ivanov, Yuan Tian, Andrey V. Dobrynin, and Sergei S. Sheiko. "Independently Tuning Elastomer Softness and Firmness by Incorporating Side Chain Mixtures into Bottlebrush Network Strands." *Macromolecules* 53, no. 21 (2020): 9306-9312.

5.   Vatankhah-Varnosfaderani, Mohammad, William FM Daniel, Matthew H. Everhart, Ashish A. Pandya, Heyi Liang, Krzysztof Matyjaszewski, Andrey V. Dobrynin, and Sergei S. Sheiko. "Mimicking biological stress–strain behaviour with synthetic elastomers." *Nature* 549, no. 7673 (2017): 497-501.

6.   Urayama, Kenji, Takashi Miki, Toshikazu Takigawa, and Shinzo Kohjiya. "Damping elastomer based on model irregular networks of end-linked poly(dimethylsiloxane)." *Chemistry of materials* 16, no. 1 (2004): 173-178.

7.   Vatankhah-Varnosfaderani, Mohammad, Andrew N. Keith, Yidan Cong, Heyi Liang, Martin Rosenthal, Michael Sztucki, Charles Clair et al. "Chameleon-like elastomers with molecularly encoded strain-adaptive stiffening and coloration." *Science* 359, no. 6383 (2018): 1509-1513.

8.   Dalsin, J.; Hillmyer, M. A.; Bates, F. S. Linear Rheology of Polyolefin-Based Bottlebrush Polymers. *Macromolecules* **2015,** *48* (13), 4680–4691.

9.   Chen, X.; Stadler, F. J.; Larson, R. G. Method for obtaining tube model parameters for commercial ethene/α-olefin copolymers. *Journal of Rheology* **2010,** *54* (2), 393-406.

10.   Liang, Heyi, Benjamin J. Morgan, Guojun Xie, Michael R. Martinez, Ekaterina B. Zhulina, Krzysztof Matyjaszewski, Sergei S. Sheiko, and Andrey V. Dobrynin. "Universality of the entanglement plateau modulus of comb and bottlebrush polymer melts." *Macromolecules* 51, no. 23 (2018): 10028-10039.

11.   Liang, Heyi, Zhen Cao, Zilu Wang, Sergei S. Sheiko, and Andrey V. Dobrynin. "Combs and Bottlebrushes in a Melt." *Macromolecules* 50, no. 8 (2017): 3430-3437.

CHAPTER III

SYNTHESIS OF ACRYLATE ELASTOMERS

3.1 Acrylate Monomers for Advanced Elastomer Architectures

Linear elastomers are currently used in synthetic soft tissues because they can closely mimic the initial modulus of their corresponding native tissue counterparts. However, when mechanically strained linear elastomers fail to match the strain stiffening behavior of their native tissue counterparts, whose stiffness increases exponentially at small strains. Bottlebrush elastomers can be soft, yet highly strain stiffening, while also efficiently dampening mechanical vibrations at high frequencies. Previously, we found that varying the crosslink density of in bottlebrush elastomers allows for a high degree of control of the materials modulus and shows a strong agreement with theory.[1] Now, we present a series of bottlebrush and comb elastomers with both varied sidechain length and crosslink density. These materials have widened the scope of accessible mechanical properties compared with our previously synthesized elastomers due to the ability to change the sidechain length in addition to the crosslink density. These materials show promising mechanical properties for dielectric elastomer devices.

In general, many of the commonly used methods for synthesizing bottlebrush and comb macromolecules yield polymer melts using some sort of controlled free radical polymerization.[2-5] Previously, synthesized elastomer have also followed a similar approach with the development of ABA block copolymer elastomers combining a linear A block with a brush or comb like B block.[6-7] Solvent evaporation of a solution containing these polymer yields an elastomer film

where the A block is separated into spherical domains connected by polymer brushes. Another simple approach, uses readily avaliable PDMS macromonomers and crosslinker, which are then polymerized together to form a chemically crosslinked elastomer network.[8] However, all of these systems have the distinct disadvantage because the backbone of the polymer brush does not chemically match that of the sidechains. This mismatch in chemical properties can make it difficult to conduct more fundamental studies into graft polymer architectures. This work hopes to expand on these previously published methods to create graft polymer architectures that do not contain chemically different backbone monomers compared to their sidechains.

The synthetic system presented here is made from cheap and readily accessible acrylate monomers. The general, approach first uses ATRP to short synthesize PBA oligomers using a monofunctional ATRP initiator. After this, a simple one-step reaction is used to displace the terminal bromine of the oligomer with a methacrylate group. This yields a PBA macromonomer with a narrow sidechain distribution and high chain end functionality. A similar procedure is also used to synthesize PBA crosslinker, but in this case a difunctional ATRP initator used, so that after functionalization a methacrylate functional group is added to both ends of the polymer chain. Once both the macromonomer and crosslinker are made they are combined with a free radical UV initiator and varied amount of BA spacer to synthesize elastomer films.

These films have graft polymer architectures and it is straight forward process to make a variety of different architectures. Using little to no PBA macromonomer will yield an elastomer which has a linear type architecture, whereas using a moderate to high amount of PBA macromonomer will yield an elastomer with a comb and bottlebrush architecture respectively (Figure 3.1A). By incorporating more sidechains into the elastomer this should result in a physical separation. Figure 3.1B shows the detailed network architecture. The sidechain length of

the PBA macromonomer is directly related to the network parameter n_{sc}. The crosslink density, n_x, is controlled by the ratio of macromonomer and spacer to the amount of added crosslinker. The grafting density n_{sc}. The grafting density, n_g, is the average number of spacer per PBA macromonomer added plus the additional backbone monomer for the sidechain. Another unique control parameter of this system of the degree of polymerization of the crosslinker molecule and this will be referred to as n_c.
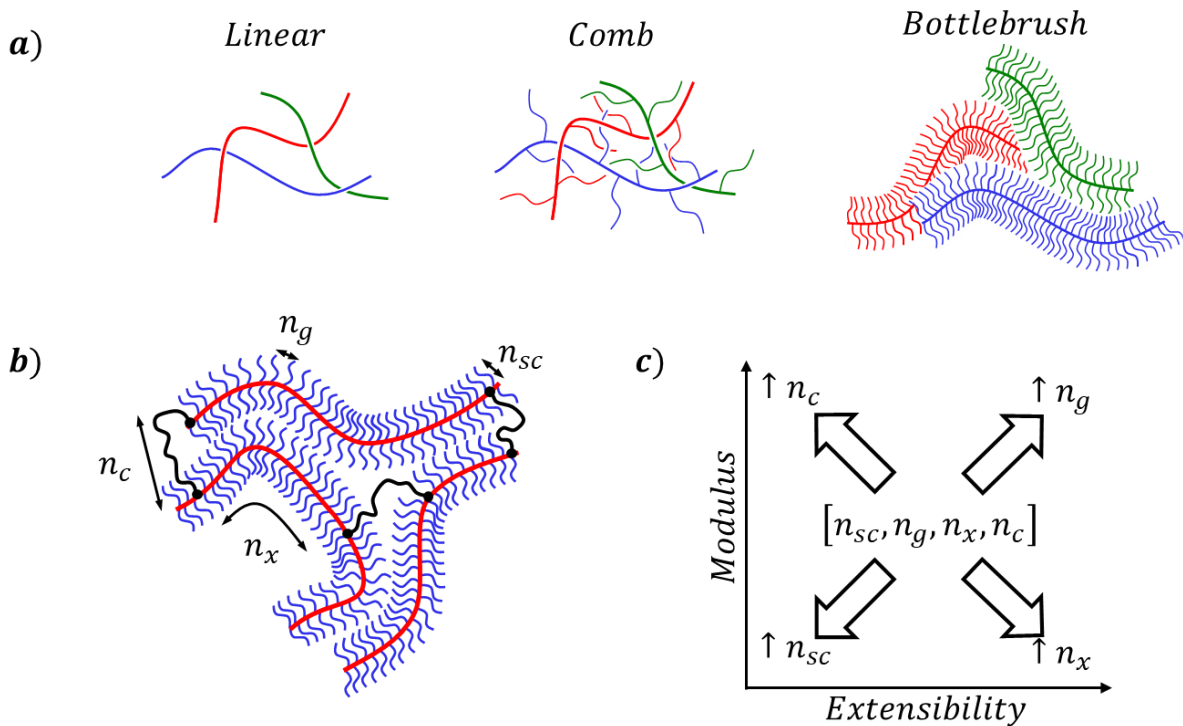
Figure 3.1: Poly(butylacrylate) graft polymer model system. (**A**) The transition between linear, combs, and bottlebrush polymers in the melt increases the separation between backbones. (**B**) Polymer architecture for the theoretical models system showing the architectural control parameters$[n_{sc}, n_x, n_g, n_c]$. (**C**) The effects of each of the architectural control parameters on the synthesized elastomers material properties. A short $n_c < n_{sc}$ will have poor incorporation to the polymer network lowering the materials modulus and increasing its extensibility.

These three network parameters can be combined in multitude of unique network architectures yield a variety of mechanical properties. In **Figure 3.1c**, it can be seen that increasing n_{sc} will in general decrease the materials modulus while also increasing its strain stiffening behavior. Increasing the n_g results in a smaller physical separation between polymer backbones and higher concentration of mechanically active strands. This leads to an overall increase in the materials modulus and extensibility. Increasing the n_x of the elastomer results in decrease in the materials overall modulus and provides a corresponding increase in the materials extensibility. The control parameter n_c is especially important for this system because it ultimately controls network homogeneity. Specifically are three cases which are $n_c < n_{sc}$, $n_c >$ n_{sc}, and $n_c \gg n_{sc}$. In the case where $n_c < n_{sc}$ crosslinker incorporation can be low especially in the case of small grafting densities and will often result in a low gel fraction a higher n_x than what should be expected by the specific architectures chemistry. For $n_c > n_{sc}$ crosslinker incorporation is generally good and the mechanical properties will better reflect the chemistry of the individually added constituents. However, in the case of $n_c \gg n_{sc}$ entanglements can be introduced into the network, which are not generally desirable for applications where graft polymer architectures are preferred to traditional linear elastomers.

3.2 Synthesis of Macromonomers and Crosslinker

Materials. 1,6-Hexanediol dimethacrylate (>90%), Phenylbis(2,4,6-trimethylbenzoyl)phosphine oxide (BAPO, 97%), Ethyl α-boromoisobutyrate (EBiB, 98%), Ethylene bis(2bromoisobutyrate) (2-BiB, 97%), copper(II) bromide (CuBr$_2$, 99.999%) *tris*[2-(dimethylamino)ethyl]amine (Me$_6$TREN), methacrylic acid (99%) and potassium tert-butoxide

(Potassium t-butoxide, 98%) were used as received from Sigma Aldrich. N-butyl acrylate (n-BA, 99%) was obtained from Sigma Aldrich and purified by passing through a column of basic alumina (Sigma Aldrich, activated, basic, Brockman I) to remove MEHQ inhibitor. Acetonitrile, anhydrous methanol, dichloromethane, acetone, anisole, and N,N-dimethylacetamide were used as received from Simga Aldrich.

Potassium methacrylate is a critical component for the functionalization of the short oligomer chains and was found to be of higher quality when synthesized in lab instead of purchasing. Approximately 25 g of potassium methoxide (0.36 mol) was dissolved in 50 mL of cold methanol in a sealed 250 mL round bottom flask equipped with a stir bar. An equal molar portion of methacrylic acid (30.68 g, 0.36 mol) was added dropwise over the course of 10 minutes stirring in an ice bath generating a white potassium methacrylate precipitate. The reaction mixture was then shaken vigorously for 5 minutes and left to equilibrate to room temperature overnight. The precipitate was separated by passing the mixture through a porous glass filter and washed immediately with an addition 25 mL of anhydrous methanol. Solvent was removed under vacuum and the potassium methacrylate was stored for later use.

Butyl acrylate macromonomers were synthesized by SARA ATRP followed by a post polymerization functionalization displacing the bromine end group with potassium methacrylate. Scheme 3.1 shows the general synthetic route that was used to synthesize these macromonomer. It is important to note that butyl acrylate is not the only material this synthesis has been used for. It has also been used to successfully make ethyl acrylate elastomers as well.
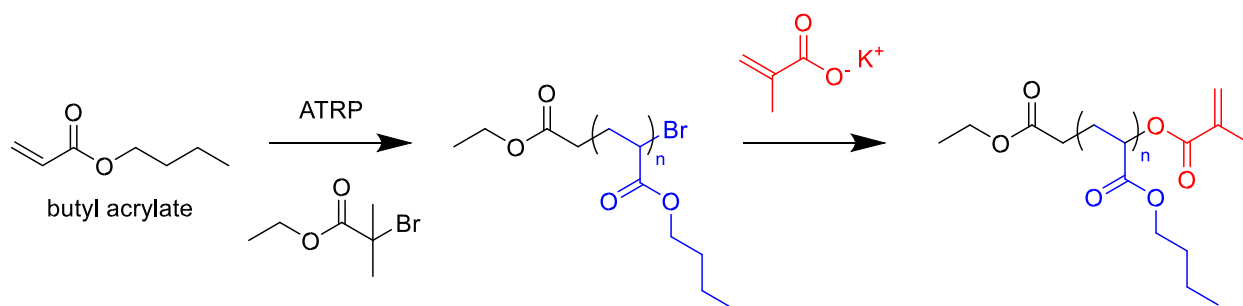
Figure 3.2: Reaction scheme for the polymerization and functionalization of macromonomers. The initial synthesis of the butyl acrylate oligomers was conducted in large 120 g batches

with the intention to stop the polymerization at 80% to yield 100 g of the PBA oligomer. To a

500 mL air free Schlenk flask 120 g of butyl acrylate was combined with Me_6TREN (10 μL),

$CuBr_2$ (8 mg), and EBiB (15.2, 7.3, or 4 g) and diluted with an equal volume of acetonitrile. The

reaction mixture was the cool with an ice bath and oxygen was removed by bubbling nitrogen

gas for 1 hour. The polymerization was initiated by adding a stir bar equipped with a clean Cu

wire and transferring to 45 C mineral oil bath. Specifically, 10 cm segment Cu wire was wrapped

around a magnetic stir bar and stirred in 10 M HCl for 5 minutes before adding to the reaction

flask. The reaction was monitored by ^1H NMR and stopped near 80% completion with the

addition of chloroform. Excess catalyst was removed by washing in water ~11 times and excess

solvent was removed by rotary evaporation at 45 C under reduced pressure. Figure 3.2 shows the

NMR spectra of the synthesized butyl acrylate oligomer with a target DP of 10. The extent of

reaction was measured to be 84% conversion, which resulted in a oligomer with a DP of 10.
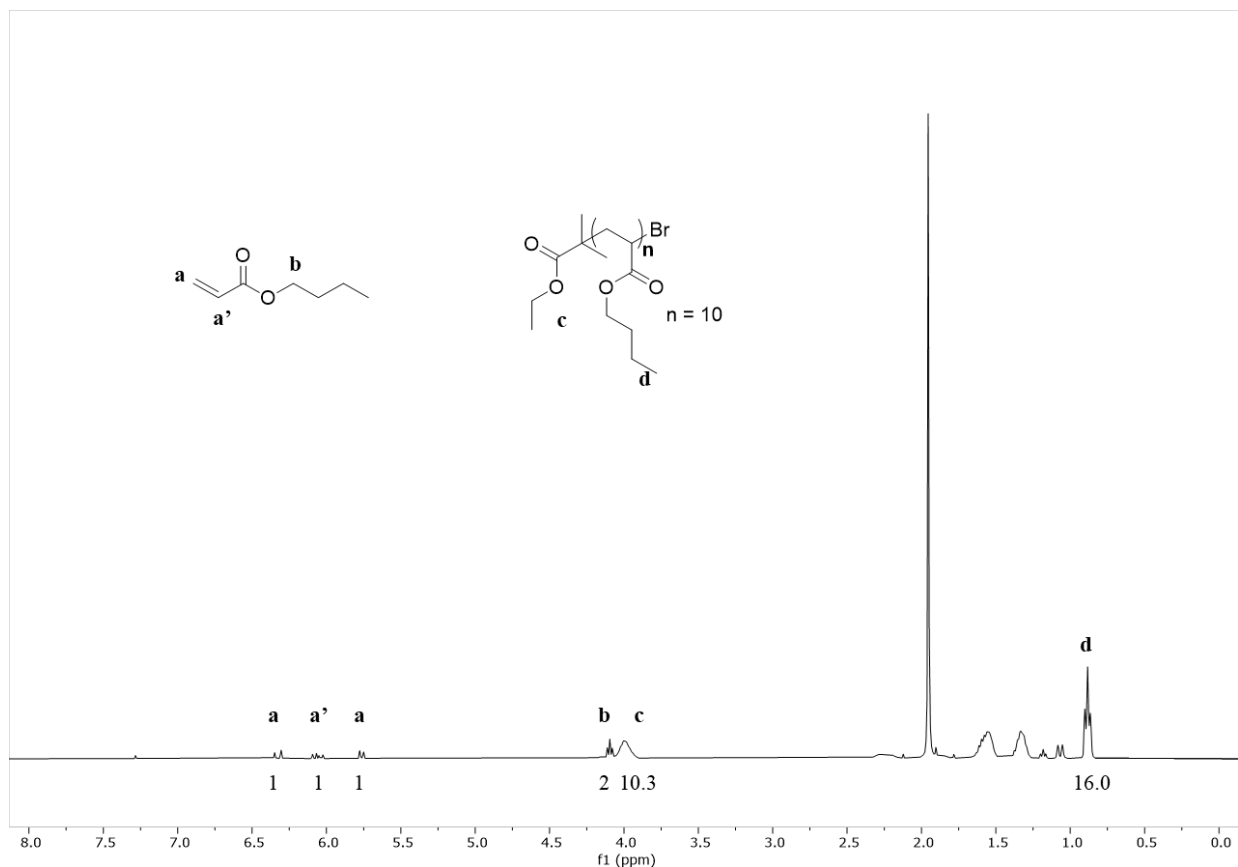
Figure 3.3: ^{1}H-NMR of unpurified butyl acrylate at completion of ATRP reaction. (400 MHz, CDCl$_3$): 6.3, 5.77 (**CH$_2$**=C(H)C=O, d, 1H), 6.06 (CH$_2$=C(**H**)C=O, dd, 2H), 4.1 (-O-**CH$_2$**-(CH$_2$)$_2$-CH$_3$, t, 2H) 4.00 (O-**CH$_2$**-(CH$_2$)2-CH$_3$, s, 10.3H), 0.88 ((-O-CH$_2$-(CH$_2$)$_2$-**CH$_3$**, t, 16H). The extent of reaction was taken to be the area ratio of peak $c/(b + c) = 0.84$.

The PBA oligomers were then functionalized by displacing the terminal bromine found on the growing chain end with potassium methacrylate to yield the PBA macromonomer. It is important to note that because the macromonomer was synthesized by ATRP the bromine group at the end of the chain must all be removed because this group will undergo side reactions with free radicals during elastomer synthesis.

The previously synthesized butyl acrylate was dissolved in 7 parts N,Ndimethylacetamide. Potassium methacrylate was added in large excess (>3 molar

equivalents) and the reaction was left to stir for 3 days and turning a faint yellow color. After each day after the first addition an addition 1 molar equivalent of potassium methacrylate was added. To purify, the mixture was 1 part chloroform and 1 part water were added separating the mixture into two separate phases. The aqueous phase was discarded and the remaining organic component was an addition 11 times with water until clear. Solvent was removed by bubbling compressed air through the polymer solution for 2 days. It is important that bubbling air is used in this case because bubbling with nitrogen often lead to spontaneous polymerization of the macromonomer. It was also found that removal of solvent using a rotary evaporator could also lead to the spontaneous polymerization of the macromonomer in some cases. Figure 3.3 shows the NMR spectra for the synthesized butyl acrylate macromonomers. The percent of functionalized percent of oligomers can be calculated by the integration of the peak at 0.88 ppm, which is labeled as d in the figure. The resulting synthesis for yielded three macromonomers with a sidechain length of 41, 23, and 11, which were found to be 95-97% functionalized.
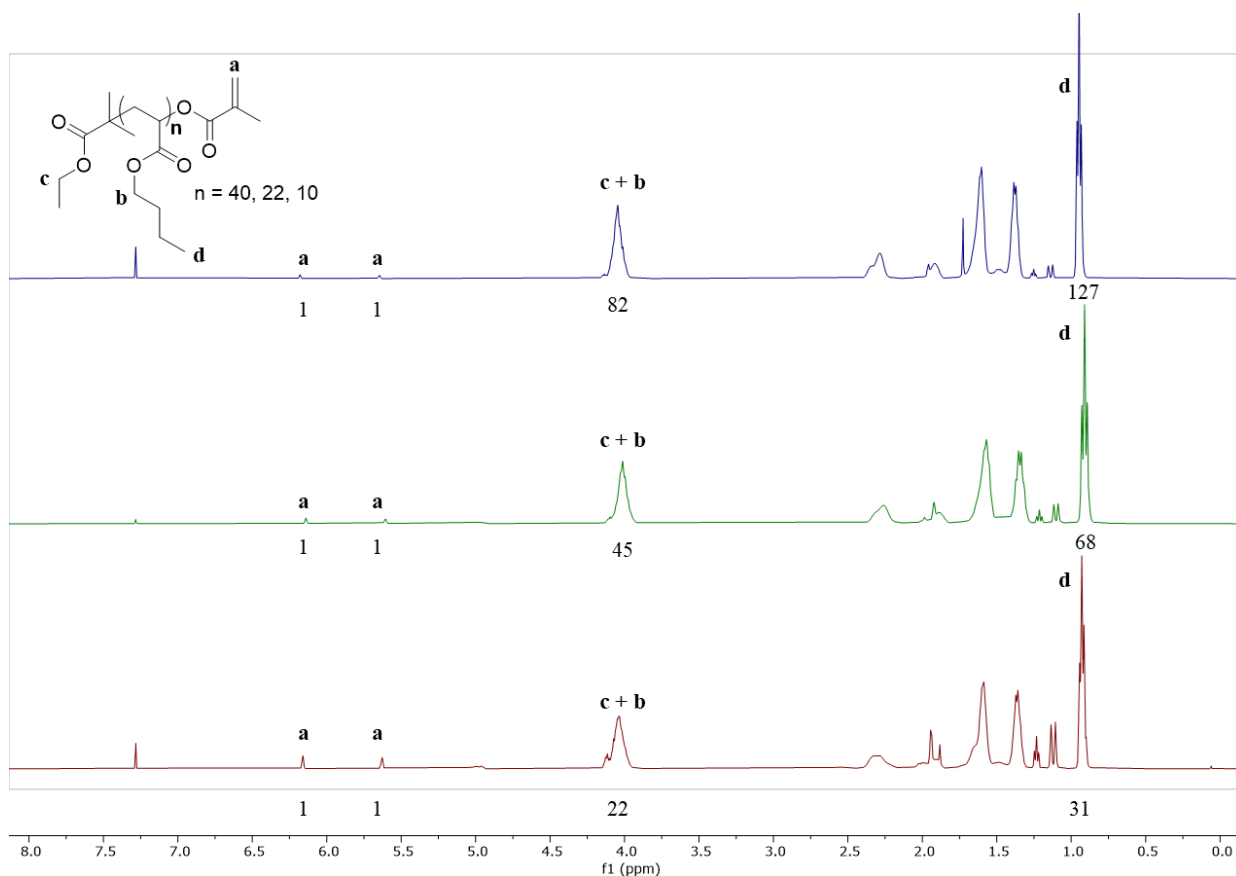
Figure 3.4: ¹H-NMR of functionalized macromonomer. (400 MHz, CDCl₃): 6.14, 5.60 (CH3-
CH2=CC=O, s, 1H), 4.01 (-O-**CH₂**-(CH₂)₂-CH₃, s, 43H) 4.01 (O-**CH₂**-CH₂, s, 2H), 0.88 ((-O-CH₂-(CH₂)₂-
CH₃, t, 67H). The synthesized oligomer starting material is shown in the upper left corner of the plot,
where n corresponds to the degree of polymerization of the starting material. The percentage of
functionalized elastomers was taken to be found to be 94.5, 97.1, and 96.8% for the oligomers with a DP of
40, 22, and 10 respectively.

Figure 3.4 shows the GPC chromatograph for the synthesized macromonomers and shows

that they have narrow molecular weight distributions. There is small peak just after 18 min in

each plot, which corresponds to a solvent impurity and is not a result of any side reaction or

unreacted oligomer in the macromonomers. However, because the difference in molecular

weight is small between the oligomer and the functionalized macromonomer it most likely

impossible to discern the difference between the two chemical species from the GPC data. The

synthesized macromonomers have been summarized in Table 3.1 below.
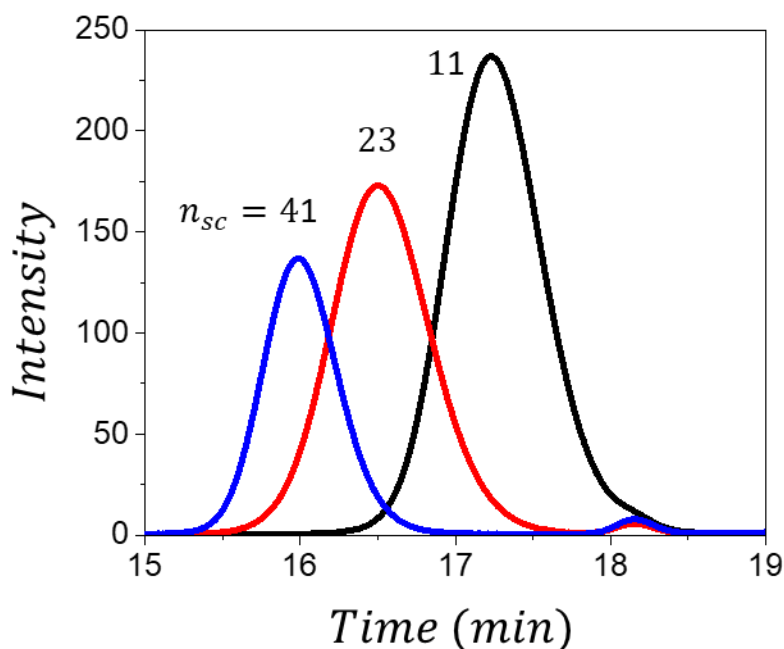
Figure 3.5: Gel permeation chromatographs of the synthesized macromonomers. The dispersity of the corresponding macromonomers was found to be 1.12, 1.08, and 1.07 for the corresponding $n_g = 11$, 23, *and* 41.

Table 3.1: PBA macromonomer

n_{sc1}	M_n (g/mol)[2]	DP[3]	% Func.[4]	Đ[5]
41	5,300	40	95	1.07
23	3,000	22	97	1.08
11	1,500	10	97	1.07

[1] The value of n_{sc} is derived primarily from the degree of polymerization of the sidechain during the initial ATRP reaction plus the additional monomeric unit from the initiator. [2] The molecular weight of the total functionalized initiator. [3] The degree of polymerization of the non-functionalized PBA oligomer. [4] The percent functionalization calculated by H[1] NMR. [5] The dispersity of the functionalized macromonomers from the GPC chromatograph in **Figure 3.4**

PBA crosslinker was also synthesized in a similar fashion to the ATRP macromonomer.

Instead of using EBiB as an initator, 2-BiB was used instead. In this way once the oligomer is

synthesized there is a bromine atom at each end of the growing chain that is displaced by the

potassium methacrylate when it is functionalized. For example, the $n_{sc} = 80$ crosslinker was synthesized by combining 24 g (0.19 mol) of butyl acrylate, Me6TREN (2 μL, 7.4 μmol), CuBr2 (1.6 mg, 7.2 μmol), and 2-BiB (0.67 g, 1.9 μmol) and diluting the mixture to 50% with acetonitrile. The reaction was then cooled in an ice bath and degassed for 1 hour with bubbling nitrogen gas. The polymerization was initiated by the addition of a Cu0 wire and transferred to a 45 C oil bath until the reaction reached ~80% conversion. The reaction was then terminated by the addition of 50 mL of chloroform and washed 11 times in water. Solvent was removed by rotary evaporation at 45 C under reduced pressure. The cleaned polymer was then functionalized by the addition of 7 parts N,N-dimethylacetamide and a large excess of potassium methacrylate and left stirring for 72 hours. 50 mL of chloroform and 100 mL of water were then added separating the polymer into the organic phase. The organic phase was then washed in water 11 times until it became clear. Solvent was again by bubbling with oxygen gas.

3.3 Synthesis of Elastomers

Three different kinds of elastomers were synthesized during this study. There were linear, comb, and bottlebrush elastomers. The linear elastomers were synthesized using only a 1,6-Hexanediol dimethacrylate crosslinker and butyl acrylate. The comb elastomers used crosslinker, PBA macromonomer, and butyl acrylate as a spacer. The bottlebrush elastomers were synthesized using primarily PBA macromonomer and crosslinker, but in some cases a small amount of spacer molecule when it was required.

Linear elastomers were synthesized by mixing 4 g n-BA, 1,6-Hexanediol dimethacrylate (1, 0.5,0.25 mol%), and BAPO (12 mg) followed by diluting the solution to 50% with anisole. The mixture was degassed with bubbling nitrogen for 1 hour and then injected in 1.3 mm thick molds and left to polymerize under ambient light conditions in a nitrogen atmosphere. After 24

hours the samples were removed from their molds and wash 3 times in toluene. Prior to washing a small chunk of the crude elastomer was separated from the sample and the gel fraction was measured. Gel fractions were measured by washing small sections of unwashed films in toluene 3 times over the course of 72 hours. The mass post washing divided by the mass of the gel fraction after washing was taken to be the gel fraction.

Butyl acrylate comb elastomers were synthesized by combining PBA macromonomer, nBA crosslinker (1, 0.5, and 0.25 mol%), BAPO (5-10 mg), and n-BA spacer. The mixture was purged of oxygen using bubbling nitrogen gas and injected into a 1.3 mm molds and left to polymerize under ambient light conditions under a nitrogen atmosphere. As a specific example, for an [11,10,100] sample, $[n_{sc}, n_g, n_x]$ 4 g of $n_{sc} = 11$ macromonomer, 3g n-BA spacer (9 molar equivalents), 0.0339 g (0.05 molar equivalents), and 5 mg of BAPO were used. A small portion of the film was removed to measure the gel fraction and the bulk part of the elastomer was washed 3 times in toluene and dried prior to sample measurement.

Butyl acrylate bottlebrush elastomers were synthesized by combining PBA macromonomer (4 g), n-BA crosslinker (1, 0.5, and 0.25 mol%), and BAPO (1-5 mg) were diluted to 50% in anisole (Figure 3.4). Nitrogen gas was used to purged with oxygen for 1 hour and then the mixture was injected into 1.3 mm thick elastomer molds and left to polymerize overnight under ambient light conditions in nitrogen atmosphere. The corresponding film was separated from its mold and a small portion was set aside to measure the samples corresponding gel fraction. The larger bulk part of the film was washed in 3 times in toluene and dried prior to measurement. Gel fractions were for the most part at or above 90%. Gel fractions were measured by washing small sections of unwashed films in toluene 3 times over the course of 72 hours. The

mass post washing divided by the mass of the gel fraction after washing was taken to be the gel

fraction.
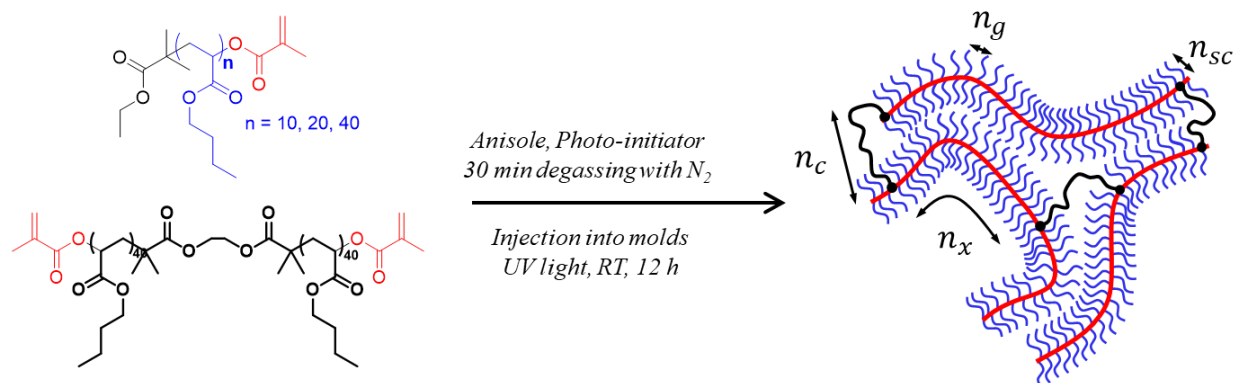
Figure 3.6: Synthesis of elastomers from macromonomer and crosslinker.

The specific molds that were used to synthesize each film were comprised of two 3 in by

4 in glass plates that 0.25 in thick and a SBR rubber spacer with a rectangle cut out of the center

(Figure 3.5). The mold was assembled by first inserting two needles through opposite sides of the

SBR rubber so that when sandwiched between the two glass plates they provide one injection

port for the mixture of monomers and another to vent the displaced gas as the liquid is injected

in. Then vacuum grease is coated onto both sides of the rubber and glass plates were attached to

either side by clamping them down with binder clips.
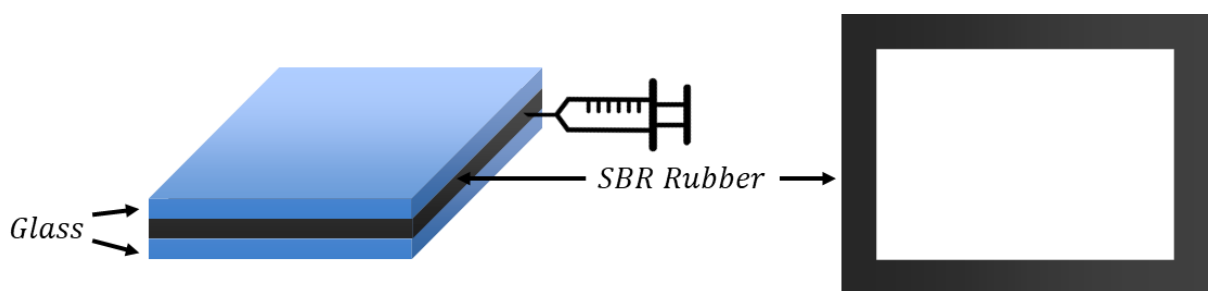
Figure 3.7: Elastomer mold design. Samples are polymerized in sealed molds comprised of two
1 mm thick glass plates separated by a SBR rubber that 1.3 mm thick. Two needles in punctured

into the sides of the rubber to allow for the mixture of macromonomer, spacer, and crosslinker to be injected into the mold.

3.4 Characterization of Elastomers

Each elastomer was characterized by measuring its gel fraction to give an estimate of network quality. A small piece of each sample was removed and dried in a 60 C oven immediately after they were removed from their molds and prior to washing with solvent. The mass of the dried film was measured after 24 hours and then the sample was washed in toluene 3 times each over a 24 hour period to allow the sample to swell to its full capacity each with each exchange of solvent. Then the film was moved over into a metal container and solvent was again evaporated in a 60 C oven overnight. The final dry mass was measured and the gel fraction was recorded as the final mass divided by the crude dry mass. In general, most films had gel fractions greater than 90% indicating that reactions ran to near completion in almost all cases. The specific gel fractions of each sample are listed in **Table 3.2**.

Table 3.2: Structural parameters synthesized elastomers

n_{sc1}	n_{g2}	n_{x3}	n_{c4}	Gel Frac. $(wt\%)^5$	G (kPa)	G_e (kPa)	β	E_0 (kPa)	Regime
1	1	50	1	98	132	42	0.11	575	Linear
		67		98	86	51	0.09	425	
		100		98	62	44	0.05	312	
		200		97	40	38	0.03	225	
11	1	50	80	97	10.3	NA	0.21	42.6	SSC
		100		95	5.6		0.15	22.6	
		200		97	2.5		0.10	11.3	
	2	50	30	94	21.4		0.20	88.3	SSC
		100		94	10.3		0.14	38.2	
		200		95	5.5		0.07	12.1	
	3	50	30	94	32.9		0.14	122	SBB

		100		95	18.9		0.10	65	
23	5	200		94	9.6		0.07	32	
		100	1	95	9.2	6.6	0.05	38.3	Comb
	5	200	1	95	3.5		0.02	21.6	Comb
	10	50	1	96	47		0.11	177	Comb
	10	67	1	97	36.9	4.8	0.08	128	Comb
	2	100	80	97	27.4	7.5	0.06	106	SSC
		200		96	15.8	7.5	0.03	69	
		50		95	12.3	NA	0.14	45.6	
23 41	2 4	100	80 30	94	5.5	NA	0.11	19.4	SSC SBB
		200		94	2.4		0.08	8.1	
		50		96	19.4		0.20	79.1	
	4 10	100	30 30	95	9.7		0.12	34.8	SBB Comb
		200		94	3.8		0.07	12.6	
		50		94	47.2		0.17	184.5	
	10 2	100	30 120	93	26.7		0.11	94	Comb SSC
		200		90	13.3		0.07	44.2	
		50		95	4.1		0.23	17.9	
41	2 5	100	120 30	95	2.2		0.11	7.8	SSC SBB
		200		88	0.7		0.06	2.3	
		25		85	13.6		0.19	46.8	
	5 10	50	30 30	84	6.1		0.15	20.4	SBB Comb
		100		84	2.4		0.09	7.7	
		25		89	36		0.16	121	
	10	50	30	88	17.4		0.15	58.1	Comb
		100		90	9.6		0.09	30.7	

[1] The value of n_{sc} is derived primarily from the degree of polymerization of the sidechain during the initial ATRP reaction plus the additional monomeric unit from the initiator. [2] The value of n_g is derived from summation the corresponding molar ratio of n-BA spacer to the macromonomer. [3] The value for n_x corresponds to the molar fraction of crosslinker compared to spacer and sidechains, where 1, 0.5, and 0.25 mol% correspond to $n_x = 50, 100, and\ 200$ respectivley. [4] n_c is the degree of polymerization of the crosslinker. [5] The gel fraction was measured by washing by washing the films in toluene and given as the mass of the washed sample as a fraction of the crude elastomer sample.

Uniaxial tensile stress strain measurements were conducted on each sample. The washed and dried films were separated out into dogbone-shaped sections using a punch with bridge dimensions of 12 mm × 2 mm × 1 mm and loaded onto an RSA-G2 DMA (TA Instruments). The samples were subjected to uniaxial extension at room temperature under a constant linear strain rate of 0.005 s^{-1}. Samples were stretched until a break occurred at the bridge. All data has been reported as a function of the True stress, σ_{true}, against elongation ratio $\lambda = L/L_0$, the length of the elongated sample normalized to the original length. The data was fitted using the relationships identified by Dobrynin *et al.*[1]

REFERENCES

1. Vatankhah-Varnoosfaderani, Mohammad, William FM Daniel, Alexandr P. Zhushma, Qiaoxi Li, Benjamin J. Morgan, Krzysztof Matyjaszewski, Daniel P. Armstrong, Richard J. Spontak, Andrey V. Dobrynin, and Sergei S. Sheiko. "Bottlebrush elastomers: A new platform for freestanding electroactuation." *Advanced Materials* 29, no. 2 (2017): 1604209.

2. Liang, Heyi, Benjamin J. Morgan, Guojun Xie, Michael R. Martinez, Ekaterina B. Zhulina, Krzysztof Matyjaszewski, Sergei S. Sheiko, and Andrey V. Dobrynin. "Universality of the entanglement plateau modulus of comb and bottlebrush polymer melts." *Macromolecules* 51, no. 23 (2018): 10028-10039.

3. Dalsin, Samuel J., Marc A. Hillmyer, and Frank S. Bates. "Linear rheology of polyolefinbased bottlebrush polymers." *Macromolecules* 48, no. 13 (2015): 4680-4691.

4. Abbasi, Mahdi, Lorenz Faust, and Manfred Wilhelm. "Comb and bottlebrush polymers with superior rheological and mechanical properties." *Advanced Materials* 31, no. 26 (2019): 1806484.

5. Tanaka, Joji, Satu Häkkinen, Parker T. Boeck, Yidan Cong, Sébastien Perrier, Sergei S. Sheiko, and Wei You. "Orthogonal Cationic and Radical RAFT Polymerizations to Prepare Bottlebrush Polymers." *Angewandte Chemie* 132, no. 18 (2020): 7270-7275.

6. Keith, Andrew N., Mohammad Vatankhah-Varnosfaderani, Charles Clair, Farahnaz Fahimipour, Erfan Dashtimoghadam, Abdelaziz Lallam, Michael Sztucki et al. "Bottlebrush Bridge between Soft Gels and Firm Tissues." ACS central science 6, no. 3 (2020): 413-419.

7. Cong, Yidan, Mohammad Vatankhah-Varnosfaderani, Vahid Karimkhani, Andrew N. Keith, Frank A. Leibfarth, Michael R. Martinez, Krzysztof Matyjaszewski, and Sergei S. Sheiko. "Understanding the Synthesis of Linear–Bottlebrush–Linear Block Copolymers: Toward Plastomers with Well-Defined Mechanical Properties." *Macromolecules* 53, no. 19 (2020): 8324-8332.

8. Vatankhah-Varnosfaderani, Mohammad, William FM Daniel, Matthew H. Everhart, Ashish A. Pandya, Heyi Liang, Krzysztof Matyjaszewski, Andrey V. Dobrynin, and Sergei S. Sheiko. "Mimicking biological stress–strain behaviour with synthetic elastomers." *Nature* 549, no. 7673 (2017): 497-501.

CHAPTER IV

MECHANICAL PROPERTY CORRELATIONS: LINEAR TO BRUSH

4.1 Introduction

Bottlebrush and comb elastomers are of unique interest due to their ability to closely mimic the mechanical properties of biological tissues without the need to add additional solvent to lower the elastomers modulus and increase the materials strain stiffening behavior.[1] In fact, it has been already shown in many different cases that if taken advantage of properly bottlebrush and comb architectures can be used to program in specific unique mechanical properties into a material in a manner that is independent of the specific monomer chemistry that is being used. This new style of approach represents a paradigm shift away from the more traditional methods used when making advanced biocompatible or biologically inspired materials.[2-6] However, the using the three independent control parameters of n_{sc}, n_g, and n_x has a serious drawback where it is difficult to control the n_x when switching between different values of n_{sc}. To put in more simple terms the extent of crosslinking in a given sample can change depending on the length of sidechains you are using and their specific grafting densities. For example, if you were to make a sample with the specific architectural parameters [11, 2,100] and then made another sample [23, 2, 100] you would expect any differences in the mechanical properties to be a direct result of the sidechain length. In reality though the degree of crosslinking between both systems actually varies greatly and there is no simple method to directly measure the extent of crosslinking present in an elastomer material.

This work will demonstrate a method of evaluating a series of elastomer materials that is independent of their specific crosslink density through the correlation of the materials structural modulus, G, and firmness parameter, β. By using this method it will hopefully lead to the better evaluation of elastomeric materials in help to expedite the development of future similar technologies.

4.2 Theory

When trying to characterize the mechanical properties of an elastomer the modulus is a powerful concept for predicting material behavior and attempting to understand its molecular architectures. This is because there is a direct relationship between the stress generated in a material and the number of mechanically active strands that hold that stress as potential energy. For a graft polymer architecture the modulus can be given as,

$$G \cong \frac{\rho k T}{M_0 n_x \left(1 + n_{sc}/n_g\right)} \qquad 4.1$$

where M_0 corresponds to monomer molecular weight, ρ is the materials density, and k corresponds to the Boltzmann constant. This equation will be referred to as a materials structural modulus from which you can start to understand more about the materials architecture by evaluating the molecular parameters n_{sc}, n_g, and n_x. However, in practice it is uncommon to measure this sort of modulus with a physical experiment.

If you take a simple stress strain uniaxial extension measurement the materials modulus is often characterized by the initial slope upon deformation (**Figure 4.1**). This is inaccurate for materials comprised of semi-flexible polymer strands like graft polymers. Materials containing semi-flexible strands often undergo a large amount of strain stiffening, which will artificially

increase the perceived modulus of the material if it is being measured as the initial slope of a
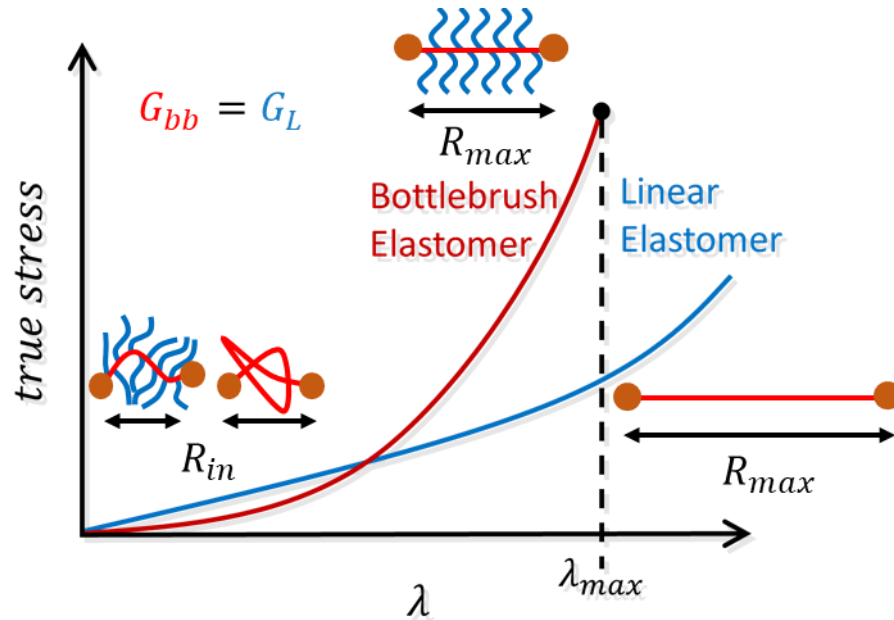
stress strain curve (**Figure 4.1**).

Figure 4.1: Stress strain curve of a linear and bottlebrush elastomer. The true stress vs elongation of a theoretical linear elastomer and bottlebrush elastomer. $\lambda = l/l_0$ corresponds to the elongation factor of the sample during a uniaxial extension experiment and is a ratio of the length of the sample in a stretched state, l, compared to its original state, l_0. In the material the length of the network strands in the non-stretched state (l_0) are given as R_{in}, but as the sample stretches to its breaking point the network strand eventually become fully stretched out to R_{max}. In the case of these two elastomers they share an equivalent structural modulus, but the apparent modulus, which is measured as the initial slope of the graph is different.

Instead it is much more accurate to use the relationship which describes the true stress generated

in a material as a function of its structural modulus, G, and the extension ratio or firmness

parameter, β.[7]

$$\sigma_{true} = \frac{G}{3} \left(\lambda^2 - \frac{1}{\lambda} \right) \left(1 + 2 \left(1 - \frac{\beta}{3} \left(\lambda^2 + \frac{2}{\lambda} \right) \right)^{-2} \right)$$
4.2

In this case $\beta = \langle R_{in}^2 \rangle / R_{max}^2$, the ratio of the mean-square average end-to-end distance of the polymer strand in an undeformed network divided by the square of the maximum end-to-end distance of the given network strand. In the case of an elastomeric material which is highly entangled, the relationship is given below.

$$\sigma_{true} = \frac{G}{3}\left(\lambda^2 - \frac{1}{\lambda}\right)\left(1 + \frac{3G_e}{G\lambda} + 2\left(1 - \frac{\beta}{3}\left(\lambda^2 + \frac{2}{\lambda}\right)\right)^{-2}\right) \qquad 4.2$$

In this expression G_e corresponds to the portion of the materials modulus that is a result of entanglement present in the material. Simple fitting of a stress strain curve can then be used to find the corresponding G and β parameters present in a given material. Incidentally the apparent modulus, G_0, which is often measured as the initial slope of a given stress strain curve is simply the derivate of equation 4.2 at $\lambda = 1$.

$$G_0 = \frac{G}{3}\left(1 + 2\left((1 - \beta)\right)^{-2}\right) \qquad 4.3$$

Now that the stress strain in a material can be simply described as a function of the materials structural modulus and firmness parameter it is imperative to draw a correlation between those two physical parameters and how they are affected by corresponding network architecture. To that end let us consider once again the structural modulus, but instead related to the number density of strands per unit volume, ρ_s.

$$G = kT\,\rho_s\,\frac{\langle R_{in}^2 \rangle}{b_k R_{max}} \qquad 4.4$$

Here, b_k corresponds to the Kuhn length of the specific graft polymer architecture and the $\rho_s = \varphi/vn_x$. Now knowing that the $\langle R_{in}^2 \rangle$ and b_k will greatly vary between different graft polymer

regimes we can start to cross correlate the measured structural parameters G and β, with the specific architectural parameters of the synthesized samples to address exactly which regime their observed mechanical properties belong to. Specifically we know that the Kuhn length b_k for each regime from **Table 2.1**.[8] The mean-square average end-to-end distance is also know to follow the worm like chain model for the SSC and SBB regime.[9]

$$\langle R_{in}^2 \rangle = \alpha R_{max}^2 \left(1 - \frac{\alpha}{2} \left(1 - exp\left(-\frac{2}{\alpha}\right) \right) \right) \qquad 4.5$$

$\alpha^{-1} = R_{max}/b_k$ corresponds to the number of Kuhn monomers for each network strand. For the comb regime $\langle R_{in}^2 \rangle = bR_{max}$. Now for the SSC and SBB regime β can simply be

$$\beta = \frac{\langle R_{in}^2 \rangle}{R_{max}^2} = \alpha \left(1 - \frac{\alpha}{2} \left(1 - exp\left(-\frac{2}{\alpha}\right) \right) \right), for\ SBB\ and\ SSC \qquad 4.6$$

and the comb regime can be describe as

$$\beta = \frac{\langle R_{in}^2 \rangle}{R_{max}^2} = \frac{b}{R_{max}}, for\ combs \qquad 4.7$$

Now with equations 4.5, 4.7, and 4.8 we can derive cross-correlations between structural modulus, G, with the firmness parameter, β, based on the specific network architectures that were used to synthesize the graft polymer elastomers (**Table 4.1**).

Table 4.1: Cross-correlations between G and β for graft polymer regimes.

Regime	Kuhn length[a], b_K	Cross-correlation
Comb	b	$G \sim \dfrac{\beta}{1 + n_{sc}/n_g}$

Bottlebrush	SBB	$bl^{-3/2}b^{-1/2}\varphi^{-1}n_{sc}^{-1/2}$	$G \sim \dfrac{n_{sc}^{1/2}\beta}{\left(1 + n_{sc}/n_g\right)^2}$
	SSC	$v^{1/2}l^{-1/2}\varphi^{-1/2}$	$G \sim \dfrac{\beta}{\left(1 + n_{sc}/n_g\right)^{3/2}}$

[a] l - bond length, b - Kuhn length of the linear polymer strand, and v - monomer volume.

4.3 Mechanical Properties

Uniaxial tension measurements were conducted on each of the samples listed in **Table 3.2**. Measured samples were punched to the required shape using a dogbone cutter with bridge dimensions of 12 mm × 2 mm × 1 mm. Each stress strain curve is reported in terms of the true stress vs. the elongation factor λ, where $\lambda = l/l_0$. Fitting of the corresponding curves was done using equations 4.2. In the case where entanglements were present in the sample to a significant extent equation 4.3 was used instead. The apparent Young's modulus was also found my measuring the slope of each curve at small strains ($\lambda < 1.1$). Each sample has been included into the diagram of states **Figure 4.2** for each series of n_{sc} a sample was chosen that falls into each regime to allow for good sample coverage.
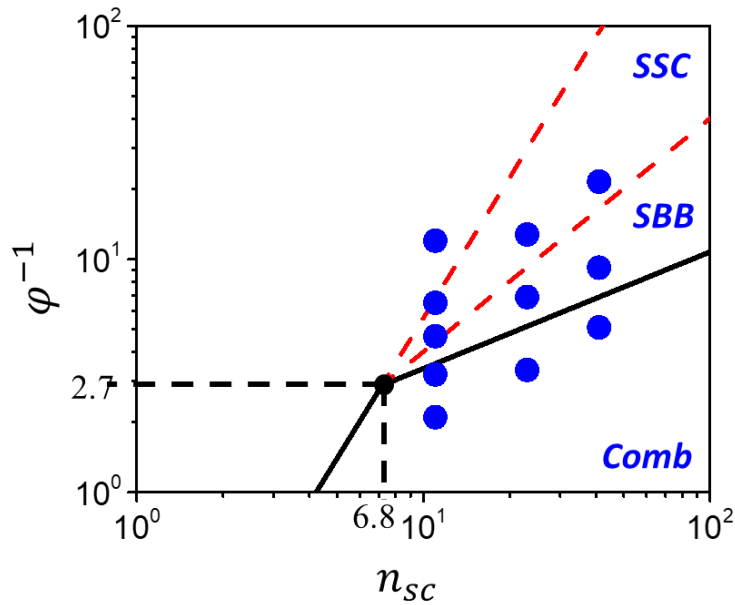
Figure 4.2: Diagram of states for PBA elastomers. True stress vs elongation curve profiles of the $n_{sc} = 11$ series of samples. The data points are shown in black, whereas the red lines correspond to the best fit line for $\sigma_{true} = G/3(\lambda^2 - \lambda^{-1})\,(1 + 2(1 - \beta/3(\lambda^2 + 2/\lambda))^{-2})$, where, G and β were the fitting parameters. **(a)** $n_{sc}=11$, $n_g = 1$. **(b)** $n_{sc}=11$, $n_g = 2$. **(c)** $n_{sc}=11$, $n_g = 3$. **(d)** $n_{sc}=11$, $n_g = 10$.

The stress strain curves for the $n_{sc} = 11$ series are shown in **Figure 4.3**. It can be seen with the exception of the [11,10] series that the stress at break for all samples ranges between 100300 kPa. It should be noted that for fitting the [11,10] series equation 4.3 was used on account of the observance of a significant number of entanglements present in the measured elastomers. This can be observed by small amounts of strain softening present at small values of λ, which is characterized by a gradual decrease of slope in the early parts of the graph. In general, it can be observed that the higher the n_g of the synthesized sample for this series, the larger the degree of strain stiffening can be observed.
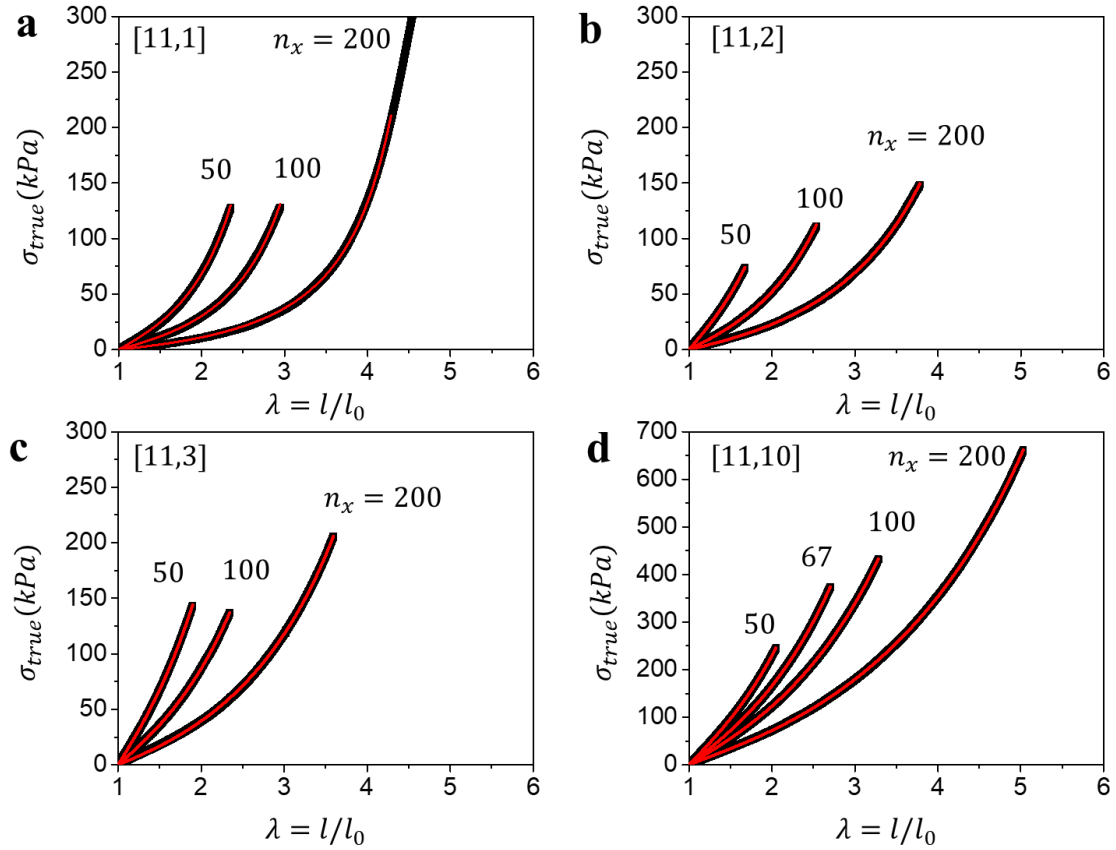
Figure 4.3: Stress strain curves for PBA $n_{sc} = 11$ series. True stress vs elongation curve profiles of the $n_{sc} = 11$ series of samples. The data points are shown in black, whereas the red lines correspond to the best fit line for $\sigma_{true} = G/3(\lambda^2 - \lambda^{-1})(1 + 2(1 - \beta/3(\lambda^2 + 2/\lambda))^{-2})$, where, G and β were the fitting parameters. **(a)** $n_{sc}=11$, $n_g = 1$. **(b)** $n_{sc}=11$, $n_g = 2$. **(c)** $n_{sc}=11$, $n_g = 3$. **(d)** $n_{sc}=11$, $n_g = 10$.

The stress strain curves for the $n_{sc} = 23$ series are shown in **Figure 4.4**. The corresponding fits for each curve accurately match the measured values from the stress train curves. Although the amount of observed strain stiffening is relatively similar between each series of samples, the modulus values obtained from fitting vary greatly. Between each increase in the grafting density the modulus of the measured samples a significant increase in the materials modulus is observed.
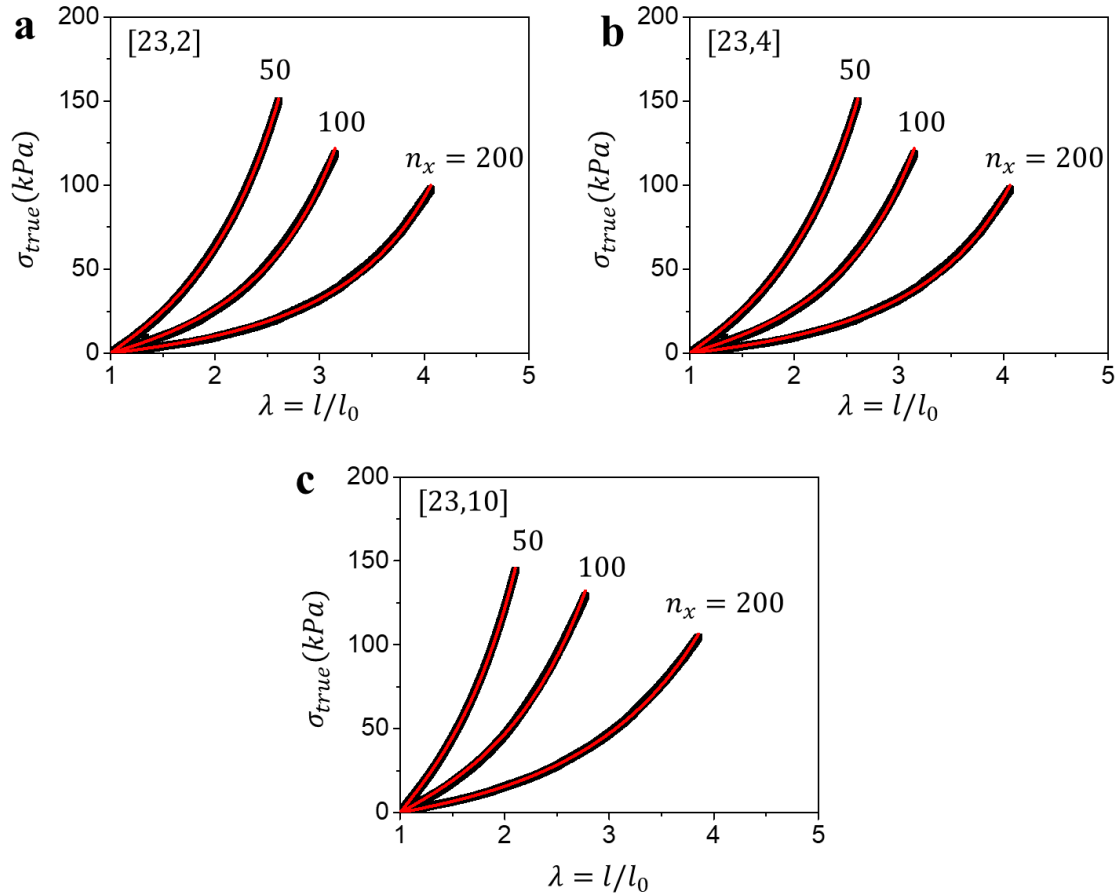
Figure 4.4: Stress strain curves for PBA $n_{sc}=23$ series. True stress vs elongation curve profiles of the $n_{sc}=23$ series of samples. The data points are shown in black, whereas the red lines correspond to the best fit line for $\sigma_{true}=G/3(\lambda^2-\lambda^{-1})(1+2(1-\beta/3(\lambda^2+2/\lambda))^{-2})$, where, G and β were the fitting parameters. **(a)** $n_{sc}=23$, $n_g=2$. **(b)** $n_{sc}=23$, $n_g=4$. **(c)** $n_{sc}=23$, $n_g=10$.

The stress strain curves for the $n_{sc}=41$ series are shown in **Figure 4.5**. Here a significant decrease in the overall stress at break is observed for the [41, 2] sample series when compared to the $n_{sc}=11$ and the $n_{sc}=23$ elastomers. The [41, 2,200] sample also shows significant levels of noise for $\lambda<4$. This noise is an artifact of the DMA instrument used to measure the sample. The measured stress values are low enough that it is possible to observe instrument noise from the motor. The structural modulus of the [41, 2,200] sample was found to be an unprecedented 700 Pa.

45

Figure 4.5: Stress strain curves for PBA $n_{sc} = 41$ series. True stress vs elongation curve profiles of the $n_{sc} = 41$ series of samples. The data points are shown in black, whereas the red lines correspond to the best fit line for $\sigma_{true} = G/3(\lambda^2 - \lambda^{-1})(1 + 2(1 - \beta/3(\lambda^2 + 2/\lambda))^{-2})$, where, G and β were the fitting parameters. **(a)** $n_{sc}{=}41$, $n_g = 2$. **(b)** $n_{sc}{=}41$, $n_g = 5$. **(c)** $n_{sc}{=}41$, $n_g = 10$.

The stress strain curves for the series of linear elastomers are shown in **Figure 4.6**.

Figure 4.6a shows a series of linear elastomers with the same backbone length between crosslinks as the graft polymers that were previously shown. **Figure 4.6b** shows a series of linear elastomers where the mass of the networks strands should be similar to the mass of network strands present in the [11,1] series. In this case, the samples were so extensible that they were not measured until the spontaneously ruptured. Each sample in this series was pulled instead until the

maximum stretching distance of the DMA was reached. Also, in both sets of linear samples

entanglements were present to a degree that was on the order of the structural modulus.

Significant strain softening can be seen in these samples if you look carefully at the beginning of
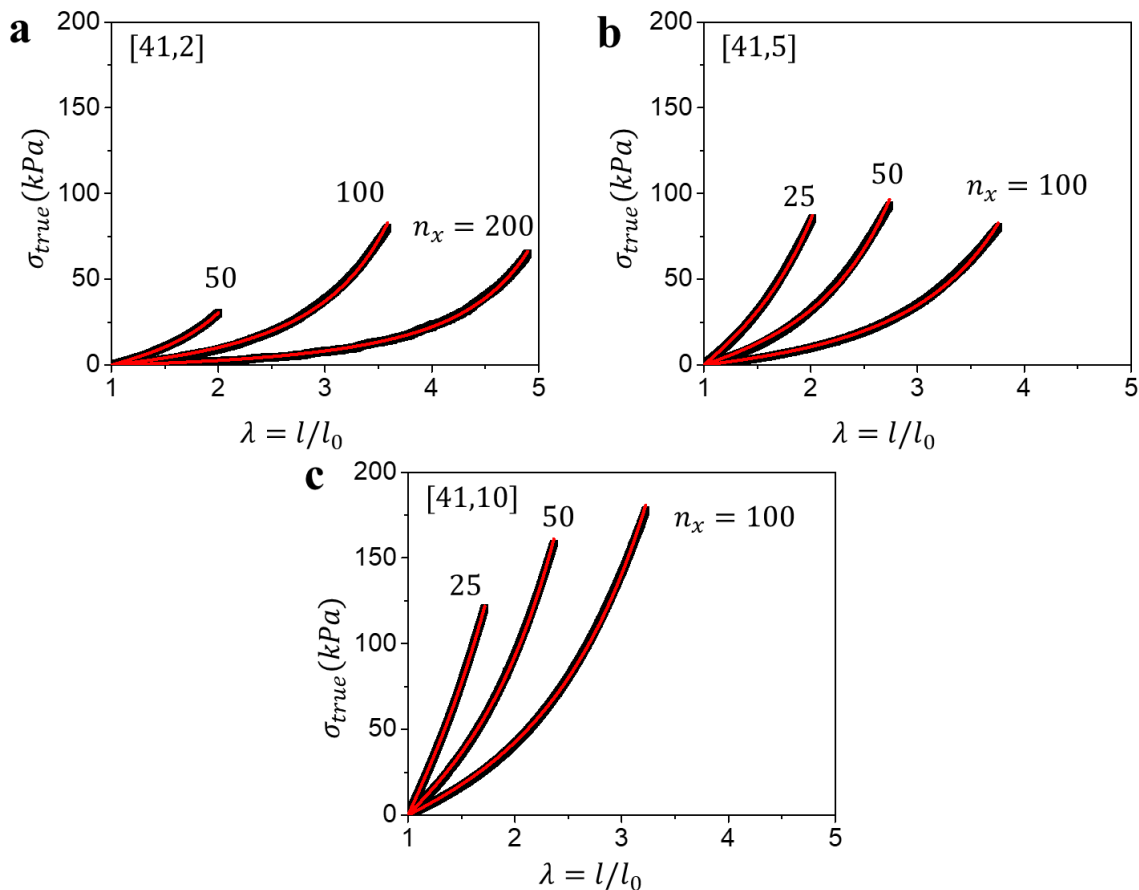
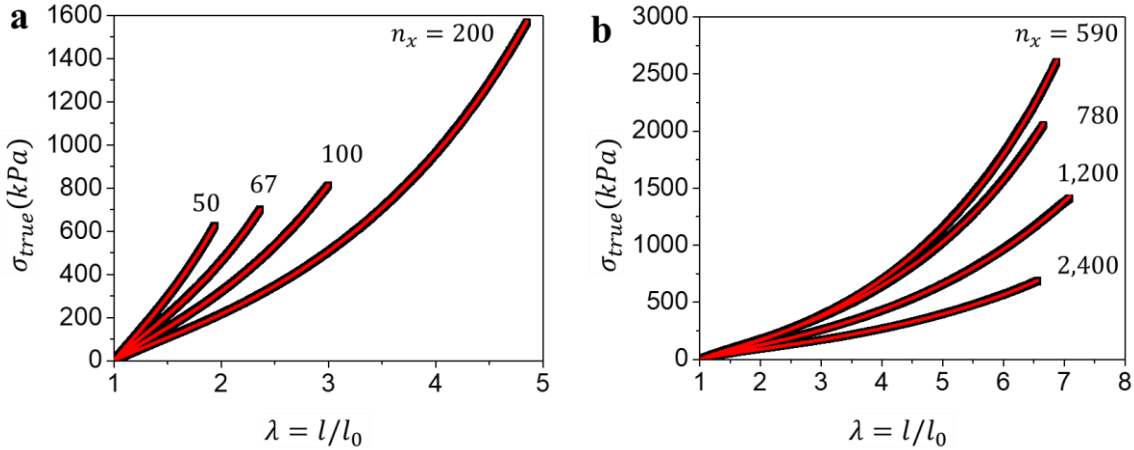the stress strain curves near $\lambda = 1$.

Figure 4.6: Stress strain curves for PBA linear elastomers. True stress vs elongation curve profiles of the $n_{sc} = 41$ series of samples. The data points are shown in black, whereas the red lines correspond to the best fit line for $\sigma_{true} = G/3(\lambda^2 - \lambda^{-1})(1 + {}^3\underline{\quad}_G\lambda^{Ge} + 2(1 - \beta/3(\lambda^2 + 2/\lambda))^{-2})$ (**a**) shows the corresponding data for linear elastomers similar backbone crosslinking densities compared to those of the studied graft polymer architectures. (**b**) Shows the corresponding linear elastomers where the mass of the crosslinked strand is similar to those of the [11,1] samples. In this case however the samples were not stretched to break because they were more extensible than the maximum stretching distance of the DMA

Compared to the linear elastomers the PBA graft polymer architectures show a significant

reduction in the structural and apparent modulus. Most significant is the [41,2] series, which

shows that the firmness parameter is more than 2x that of its linear counterparts and structural

modulus more than 40x lower the corresponding linear elastomer. This dramatic difference in the

mechanical properties is a result of a change in the materials network architecture and

completely independent of its chemical properties since they are the same. However, the challenge still exists to correlate the measured mechanical properties with the corresponding network parameters. This is because there is a difference in the n_x value you can calculate from synthesis and that which is ultimately present in the elastomer. Loops, dangles, and other defects greatly lower the crosslink density below that which can be simply describe by the concentration of crosslinking agent present during synthesis. In fact, the specific n_{sc} and n_g used during synthesis will also further change the real n_x since there is a larger steric hindrance present on the propagating chain when using large sidechain lengths and high grafting densities.

To compare the synthesized elastomers to one another a series of cross-correlations between the structural modulus and firmness ratio were derived for the Comb, SBB, and SSC regimes (**Table 4.1**). These cross-correlation relationships have been plotted with the corresponding elastomers in **Figure 4.7**. In all case we see that when each series of samples is plotted within its specific cross-correlation plot the data tends to clump together along the same line. This shows that although the crosslink density does not remain constant between different architectures it is still possible to synthesize samples of a specific G and β as long as they are chosen along these relationships.
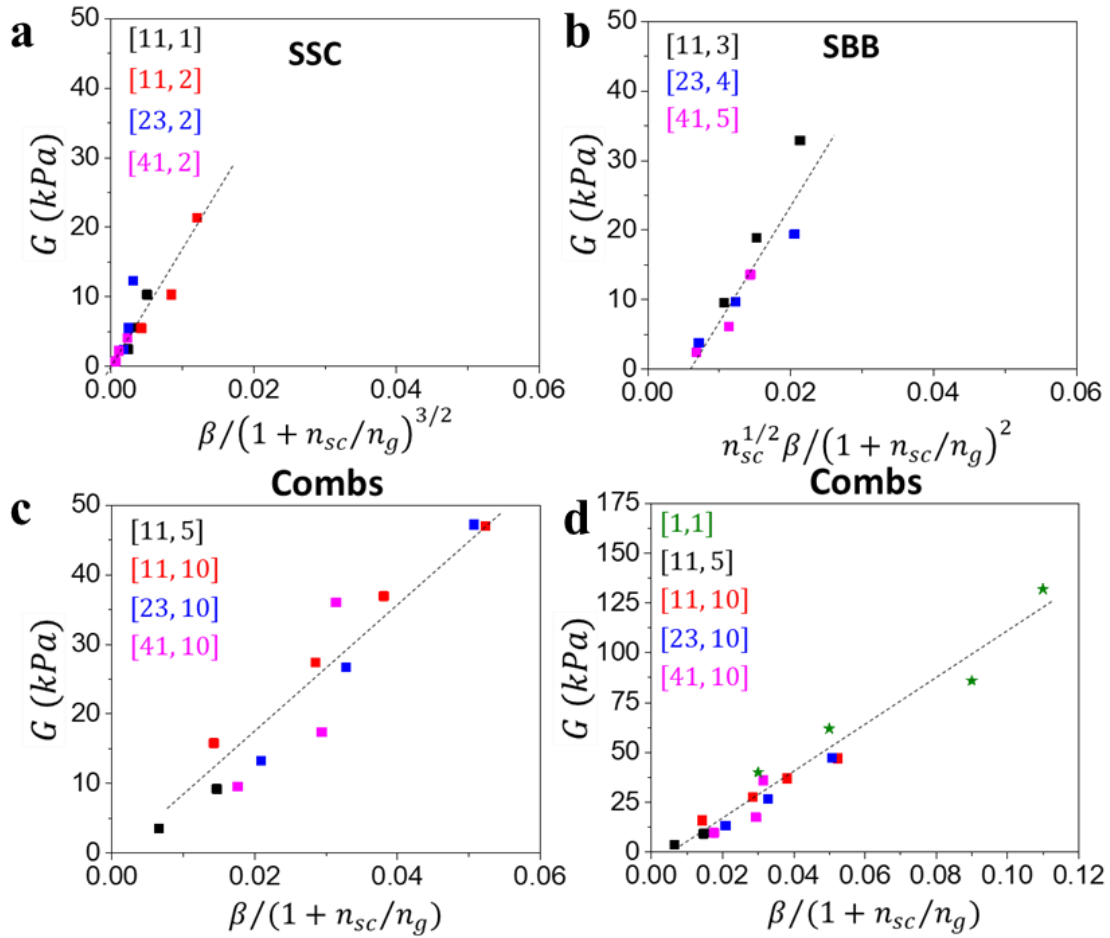
Figure 4.7: Correlation plots for PBA elastomers. The correlation plots for the corresponding PBA elastomers are shown above. (**a**) The SSC regime contains the graft polymers with the highest grafting densities. (**b**) The SBB regime containing the graft polymers with intermediate grafting densities. (**c**) The comb regime, which contains elastomers with the loosest grafting densities. (**d**) Shows an expanded comb regime going all the way to linear elastomers.

In **Figure 4.7d** it can also be seen that the comb cross correlation relationship ultimately reduces down to that of linear elastomers in the case where the sidechain length becomes sufficiently small.

REFERENCES

1. Vatankhah-Varnosfaderani, Mohammad, William FM Daniel, Matthew H. Everhart, Ashish A. Pandya, Heyi Liang, Krzysztof Matyjaszewski, Andrey V. Dobrynin, and Sergei S. Sheiko. "Mimicking biological stress–strain behaviour with synthetic elastomers." *Nature* 549, no. 7673 (2017): 497-501.

2. Griffith, Linda G., and Gail Naughton. "Tissue engineering--current challenges and expanding opportunities." *science* 295, no. 5557 (2002): 1009-1014.

3. Lv, Shanshan, Daniel M. Dudek, Yi Cao, M. M. Balamurali, John Gosline, and Hongbin Li. "Designed biomaterials to mimic the mechanical properties of muscles." *Nature* 465, no. 7294 (2010): 69-73.

4. Kim, Dae-Hyeong, Nanshu Lu, Rui Ma, Yun-Soung Kim, Rak-Hwan Kim, Shuodao Wang, Jian Wu et al. "Epidermal electronics." *science* 333, no. 6044 (2011): 838-843.

5. Green, Jordan J., and Jennifer H. Elisseeff. "Mimicking biological functionality with polymers for biomedical applications." *Nature* 540, no. 7633 (2016): 386-394.

6. Yu, Betty, Soo-Young Kang, Ariya Akthakul, Nithin Ramadurai, Morgan Pilkenton, Alpesh Patel, Amir Nashat et al. "An elastic second skin." *Nature materials* 15, no. 8 (2016): 911-918.

7. Dobrynin, Andrey V., and Jan-Michael Y. Carrillo. "Universality in nonlinear elasticity of biological and polymeric networks and gels." *Macromolecules* 44, no. 1 (2011): 140-146.

8. Jacobs, Michael, Heyi Liang, Erfan Dashtimoghadam, Benjamin J. Morgan, Sergei S. Sheiko, and Andrey V. Dobrynin. "Nonlinear elasticity and swelling of comb and bottlebrush networks." *Macromolecules* 52, no. 14 (2019): 5095-5101.

9. Rubinstein, Michael, and Ralph H. Colby. *Polymer physics*. Vol. 23. New York: Oxford university press, 2003.

CHAPTER V

SWELLING BEHAVIOR OF BRANCHED ELASTOMERS

5.1 Introduction

Biological tissues are unique class of soft materials that come from a relatively small pool of basic monomeric building blocks. Additionally, they operate under a nearly constant solvent fraction (60-80% water) biological tissues can range in modulus from $\sim 10^2$, for brain tissues, to 10^6 Pa for skin and cartilage (**Figure 5.1**).[1] When you contrast this with synthetic polymeric gels you find that this diversity of mechanical properties does not exist. For simple polymeric gels are the materials modulus is inherently linked to the solvent fraction and only by switching between different materials can the modulus of a gel remain constant for a given solvent fraction. This poses a significant restraint towards the development of new materials for reconstructive surgery and biological implants. However, taking a trial and error approach towards combining different materials together is not an efficient solution to this problem.
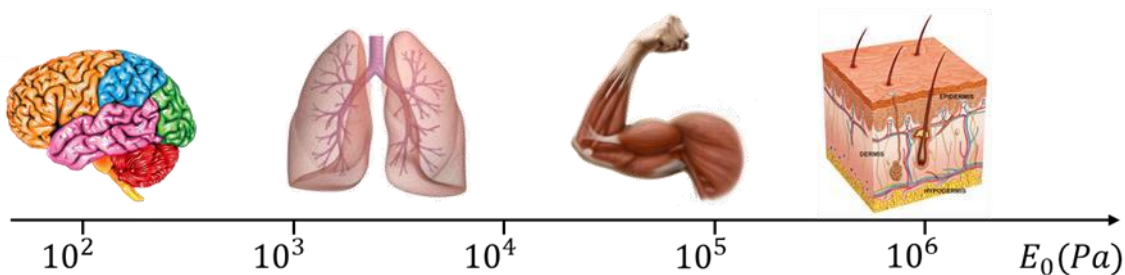
Figure 5.1: Mechanical properties of biological tissues. The approximate apparent Young's modulus of brain, lung, muscle, and skin tissues present in the human body. All these tissues are ~60-80% water by volume.

To design synthetic polymeric gels which can show a diverse range of mechanical properties at constant solvent fraction we must change their architecture. In general, equilibrium swelling ratio, Q_{eq}, is a balance between the osmotic pressure and the mechanical stress of network expansion. For a polymer network of linear polymer chains, $G \sim 1/n_x \sim Q_{eq}^{-0.57}$ in a good solvent, which means it is impossible to synthesize materials like biological gels from a single material.[2] However, graft polymer elastomers represent a unique materials design platform to serve this specific purpose. By taking advantage of architectures with network parameters n_{sc}, n_g, and n_x graft polymer gels would show a range of mechanical properties at constant solvent fractions.

5.2 Theory

For any polymer network the swelling ratio will be defined as $Q = V/V_0$, where V is the total volume of the swollen network and V_0 is the volume of the polymer without additional solvent. Since the extent of expansion is equal in all directions the deformation can be defined by the stretching factor in one dimension $\lambda_s = Q^{1/3}$. The equilibrium swelling, Q_{eq} ratio is the point at which the osmotic pressure and the mechanical stress of network expansion are in balance with one another and are characterized by the relationship,[3]

$$\frac{G_{dr}}{3}\left(1 + 2\left(1 - \frac{\beta I_1(Q)}{3}\right)^{-2}\right) = Q^{\frac{1}{3}}\pi(Q) \qquad 5.1$$

where G_{dr} is the network modulus in the dry state, $\pi(Q)$ is the osmotic pressure for any given Q, and $I_1(Q) = 3Q^{2/3} = I_1(\lambda) = \lambda^2 + 2\lambda^{-1}$ is the first deformation invariant. This relationship can also be used to describe the deformation-dependent shear modulus of a network in a swollen state, $G(Q)$.

$$G(Q) = \frac{\sigma_{true}}{\lambda^2 - \lambda^{-1}} = \frac{G_{dr}}{3}\left(1 + 2\left(1 - \frac{\beta I_1(Q)}{3}\right)^{-2}\right) \qquad 5.2$$

Using this relationship, the structural modulus and elongation ratio of a material can be extracted from the stress strain curve and then. Also, the deformation-dependent shear modulus of a swollen network has previously been defined[1] as

5.3 Swelling of PBA Elastomers

In a simple linear elastomer the equilibrium swelling ratio will also have a unique value for any given n_x of that system. This also means that for any series of linear elastomers it is impossible to decouple the swelling ratio from the materials modulus, maximum extensibility, and the corresponding mechanical properties in the swollen (**Figure 5.1a**). However, for the case of graft polymer elastomers, a myriad of architectural parameters are available such that one can truly decoupled the solvent fraction of a material from its mechanical properties (**Figure 5.1b**).
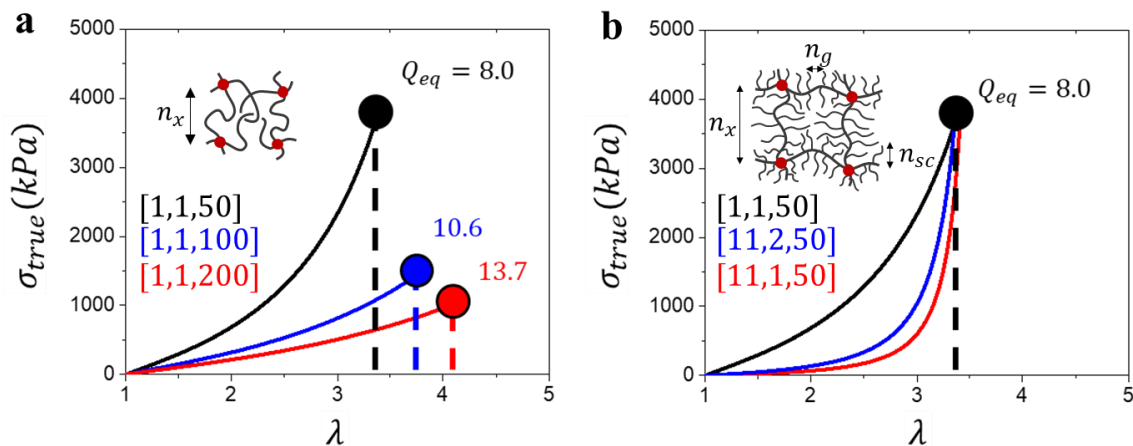
Figure 5.2: Swelling contrast in linear and graft polymer systems. Comparison between the swelling behavior of linear elastomer systems and graft polymer systems. (**a**) Shows the corresponding stress strain curves of three linear elastomers based on their measured G and β values up to the comparative λ values up to the equilibrium swelling ratio. (**b**) The stress strain curves of a linear elastomer with the same swelling ratio of two graft polymer elastomers. The curves were generated from their measured G and β values.

Figure 5.1 is a direct example of this concept. In the figure the stress strain curves were generated using equation 4.3 up until the corresponding λ value that relates the stress in the network under uniaxial extension to the stress in the network generated by the same Q_{eq} value shown. It can be clearly seen in **Figure 5.1a** from the three linear elastomers of varying crosslink density is that the equilibrium swelling ratio varies with respect to n_x and the modulus of the material. However, in the case of graft polymer elastomers (**Figure 5.1b**) it is a relatively simple matter to synthesize two different elastomers with different network architectures, such that even though the modulus of the sample is different the value of Q_{eq} is the same. This is a consequence of the decoupling of the materials swelling ratio from the modulus of the material.

This concept works because the structural modulus and firmness parameter of the synthesized elastomer ultimately dictate the equilibrium swelling ratio of a material when solvent

quality or composition of that material does not change. For linear elastomers the $G \sim n_x^{-1}$ and $\beta \sim n_x^{-1}$ and the result of this is that Q_{eq} is a unique value for each crosslink density (equation 5.1). However, the case of graft polymer elastomers $G \sim n_x^{-1}\varphi^{-1}$ and $\beta \sim n_x^{-1}n^1{}_{sc}/2$ and in this case it is possible to synthesize network architectures such that the structural modulus and firmness parameter are decoupled from one another and as a consequence so is the equilibrium swelling ratio.

To verify this results a series of PBA elastomers was synthesized and their equilibrium swelling ratio was measured by swelling in toluene for 24 hours. The corresponding swollen mass was measured and then the dry mass was measured after the sample was dried in a 60 C oven for an additional 24 hours. The Q_{eq} was given by the equation below.

$$Q_{eq} = \frac{(M_s - M_{PBA})\rho_{PBA}}{M_{PBA}\rho_s} + 1 \qquad\qquad 5.3$$

The measured swelling ratio as well as the corresponding mechanical properties of the synthesized PBA elastomer samples are reported in **Table 5.1**. The deformation-dependent shear modulus of a network in a swollen state, $G(Q_{eq})$ was then calculated by using the corresponding elastomers stress strain curves at the trues stress for the value of λ, where $3Q_{eq}^{2/3} = \lambda^2 + 2\lambda^{-1}$ and then normalizing that stress by $\lambda^2 - \lambda^{-1}$ to yield $G(Q)$. The result of these calculations is given in **Table 5.1**.

Table 5.1: Swelling properties of synthesized elastomers

n_{sc}[1]	n_g[2]	n_x[3]	n_c[4]	G (kPa)	G_e (kPa)	β	Q_{eq}[5]	$G(Q)$ (kPa)[6]	Regime
		50		132	42	0.11	8.0	335	
1	1	67	1	86	51	0.09	8.8	195	Linear
		100		62	44	0.05	10.6	104	

		200		40	38	0.03	13.7	62	
11	1	50	80	10.3	NA	0.21	7.8	234	SSC
		100		5.6		0.15	9.7	39	
		200		2.5		0.10	14.2	11	
	2	50	30	21.4		0.20	8	368	SSC
		100		10.3		0.14	12.4	115	
		200		5.5		0.07	18.2	16	
	3	50	30	32.9		0.14	8.1	126	SBB
		100		18.9		0.10	11.4	58	
		200		9.6		0.07	17.5	26	
	5	100	1	9.2		0.05	18.9	7	Comb
		200		3.5		0.02	31.5	5	
	10	50	1	47	6.6	0.11	10.2	151	Comb
		67		36.9	4.8	0.08	13.28	94	
		100		27.4	7.5	0.06	16.04	59	
		200		15.8	7.5	0.03	20.09	24	
23	2	50	80	12.3	NA	0.14	10.5	80	SSC
		100		5.5		0.11	14.4	32	
		200		2.4		0.08	23.5	14	
	4	50	30	19.4		0.20	9.7	1620	SBB
		100		9.7		0.12	14.8	89	
		200		3.8		0.07	25.0	17	
	10	50	30	47.2		0.17	9.0	462	Comb
		100		26.7		0.11	13.2	128	
		200		13.3	NA	0.07	19.2	40	
41	2	50	120	4.1		0.23	13.7	29	SSC
		100		2.2		0.11	20.6	49	
		200		0.7		0.06	38	5	
	5	25	30	13.6		0.19	10.2	783	SBB
		50		6.1		0.15	15.7	1105	
		100		2.4		0.09	26.1	38	
	10	25	30	36		0.16	8.9	258	Comb
		50		17.4		0.15	12.9	385	
		100		9.6		0.09	18.8	52	

[1] The value of n_{sc} is derived primarily from the degree of polymerization of the sidechain during the initial ATRP reaction plus the additional monomeric unit from the initiator. [2] The value of n_g is derived from summation the corresponding molar ratio of n-BA spacer to the macromonomer. [3] The value for n_x corresponds to the molar fraction of crosslinker compared to spacer and sidechains, where 1, 0.5, and 0.25 mol% correspond to $n_x = 50, 100, and$ 200 respectivley. [4] n_c is the degree of polymerization of the crosslinker. [5] Calculated from equation 5.3. [6] Calculated from equation 5.2

To study how PBA elastomers over varying n_g, n_{sc}, and n_x behave when swollen in a solvent the values of $G(Q)$ were plotted against the equilibrium swelling ratio (**Figure 5.2a**). Although the error appears to be high for the entire series of data as a whole a slope of -2.57 was measured when the points were fit to a linear curve. The slope almost exactly matches with what was found by theory, which was found to be -2.6. The error is likely due to the specific error associated with calculating $G(Q)$ using G and β from fitting the stress strain curves. This is because the stress values calculated for each samples swelling ratio is high and certainly in the limit of nonlinear extensibility. This means that any small error in the β will lead to a relatively significant error when calculating $G(Q)$.
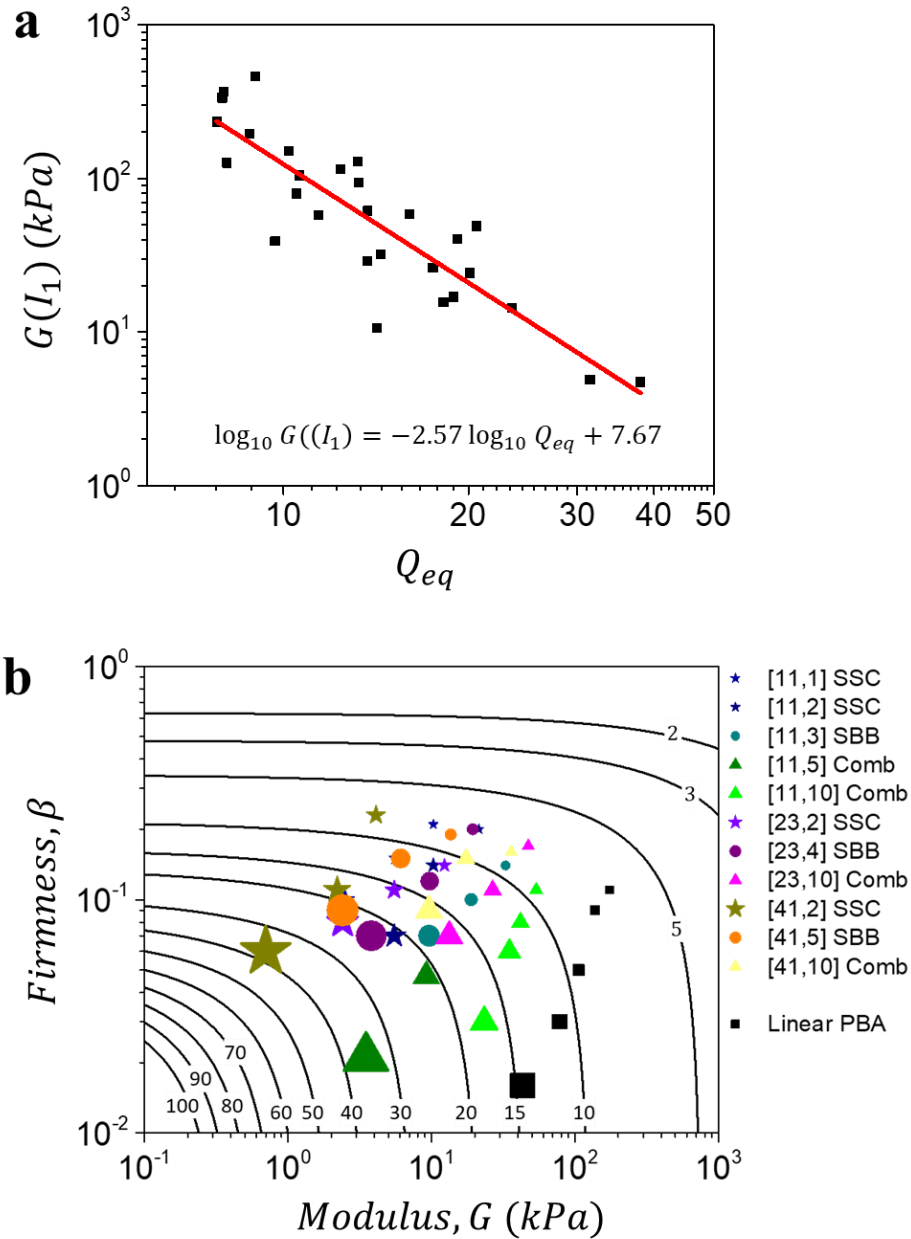
Figure 5.3: The deformation dependent shear modulus and isochoric graph of PBA elastomers. (**a**) A plot showing $G(I_1)$ against Q_{eq}. $G(I_1)$ was calculated using equation 5.2, while substituting $I_1(Q) = 3Q^{2/3}$ as the first invariant. The data was fit to a linear curve such that the equilibrium swelling ratio could be estimated for any PBA elastomer. (**b**) A plot showing the theoretical contours of the equilibrium swelling ratio as a function of G and β. In the case of when a significant amount of entanglements were present in the sample the structural modulus G was plotted as the summation of the fit parameters G and G_e. The contours were generated by using the linear fit from the proceeding plot to back calculate out the theoretical values for G and β from equation 5.2 given the label values of Q_{eq} on the contours. The data points show the actual

measured G and β for the synthesized elastomers and the relative size of the point is related to the actual swelling ratio measured for the specific elastomer. The sample data can be found in **Table 5.1**.

 Figure 5.2b shows the measured values of the firmness parameter β plotted against the structural modulus G. The individual size of each point is also changed so that it accurately reflects the relative change in swelling ratio between the samples. This means the large points on the plot correspond a larger measured swelling ratio for that sample. To help describe that trend a family of curves representing how the swelling ratio changes with respect to G and β was added and labeled with the corresponding equilibrium swelling ratio. These contours were generated by taking the fit parameters from **Figure 5.2a** and using them to back calculate the corresponding G and β that would be necessary to for each contour to satisfy equation 5.2. The resulting solutions to this equation are the contours draw. The contours appear to also be very accurate in describe the swelling ratios that were observed.

 The most important point to notice about **Figure 5.2b** is that swelling ratio of an elastomer shows a clear dependence on the structural modulus and firmness parameter. For the linear elastomers the consequence of this is that it is not possible to make a material with a different modulus that also has the same swelling ratio as another material made with the same chemical composition. However, what can clearly be seen is that this is not the case for graft polymer architectures. The modulus and firmness parameter are decoupled from one another and subsequently it is possible to make materials that at the same solvent fraction have differing mechanical properties. This closely resembles the tissues we find in biological organisms.

5.4 X-ray measurements of PBA Elastomers

To further characterize the structure of graft polymer elastomers and how that changes when they are swollen in a solvent a series of samples were sent to collaborators for ultra-smallangle x-ray scattering measurements. It has been previously seen in the literature that the distance between neighboring backbones for bottlebrush elastomers can be observed, but these measurements have not been done for combs. **Table 5.2** details the specific samples that were measured. They consist of one sample from each series of elastomers that was synthesized (**Table 5.1**). However, in the case of samples containing a low grafting density compared to the sidechain length there was not found to be a regular ordered structure to the backbone in the elastomer. This happens at a lower the grafting densities because the network strands become more flexible and eventually no longer act as ordered semi-flexible filaments.

Table 5.2: X-ray measurements of backbone spacing in PBA elastomers.

n_{sc}	n_g	n_x	φ^a	$d_1\ (nm)$	Đ^b
11	1	100	0.083	2.73	1.12
11	2	100	0.154	3.41	1.12
11	3	100	0.214	2.67	1.12
23	2	100	0.080	5.11	1.08
23	4	100	0.148	3.66	1.08
41	2	100	0.047	6.97	1.07
41	5	100	0.109	4.32	1.07
41	10	100	0.196	3.12	1.07

[a]Corresponds to the packing parameter, $\varphi = n_g/(n_{sc} + n_g)$ and is calculated based on the number of monomers on the branching sidechains and the ratio of spacer to sidechain added during synthesis. [b]Calculated by the molecular weight distribution of the sidechain macromonomers (**Figure 3.4**).

Figure 5.4 shows the intensity of scattered x-rays plotted against the scattering vector q. Here the observed peaks correspond to the distance between neighboring bottlebrush strands and the specific distance between them, d_1 was calculated by the peak position marked with in green.
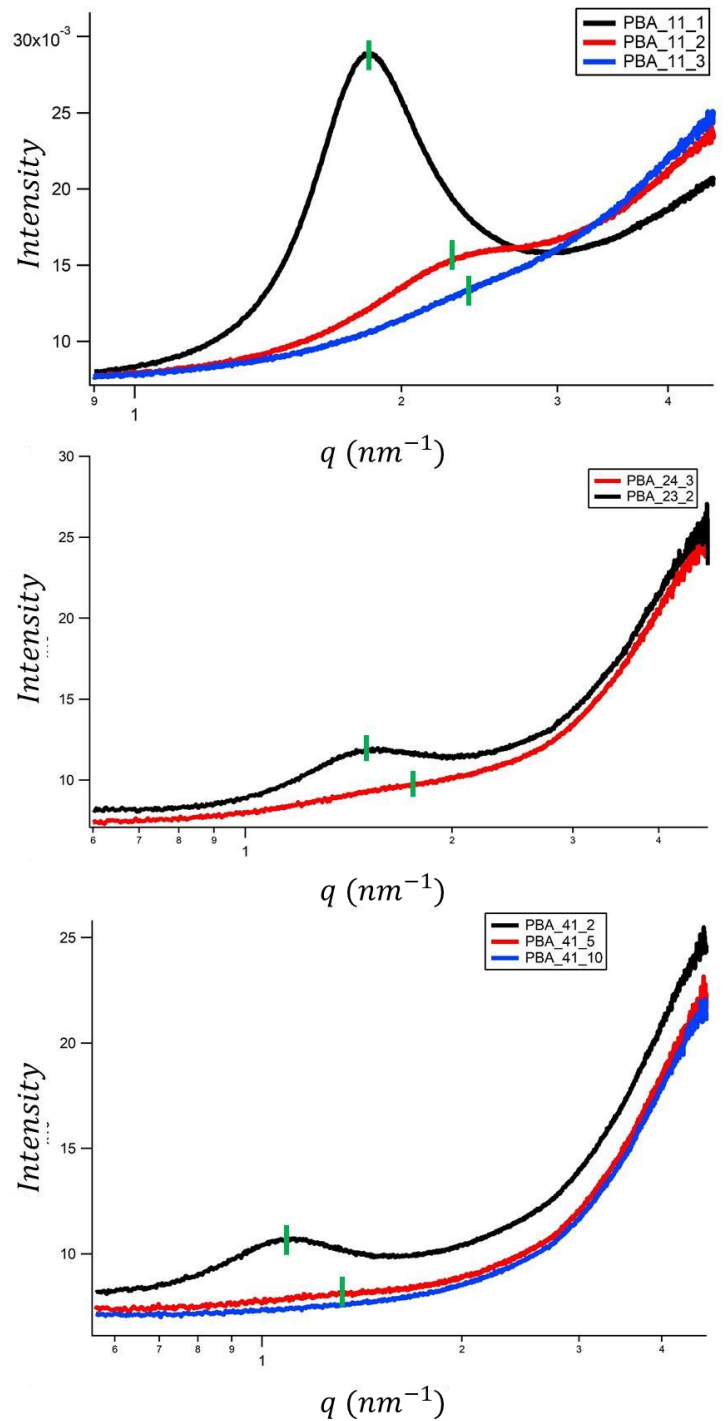
Figure 5.4: X-ray diffraction spectra of acrylate elastomers. The plots above show the intensity of x-rays plotted against the scattering vector q. The measurements are only shown for the n_g values where a peak or shoulder was seen for the d_1 spacing, which corresponds to the separation between backbones of neighboring bottlebrush and comb strands. The peak position of the d_1 peaks are shown with vertical green dashes on their corresponding spectra. The top plot shows the spectra for the n_{sc}=11 series, the middle plot shows the n_{sc}=23 series, and the bottom plot shows the n_{sc}=41 series.

Compared to the [11,1] sample many of the observed peaks are relatively small. This is because at high grafting densities of the network strand causes stearic repulsions between sidechains, which stretch out the backbone and better align them with neighboring network strands. In fact, this behavior is very similar to what happens when a polymer network is swollen in a solvent. **Figure 5.5** is similar to what is shown in **Figure 5.4**, however the [41,2] sample has been swollen in toluene and sampled every two minutes as the solvent evaporates.
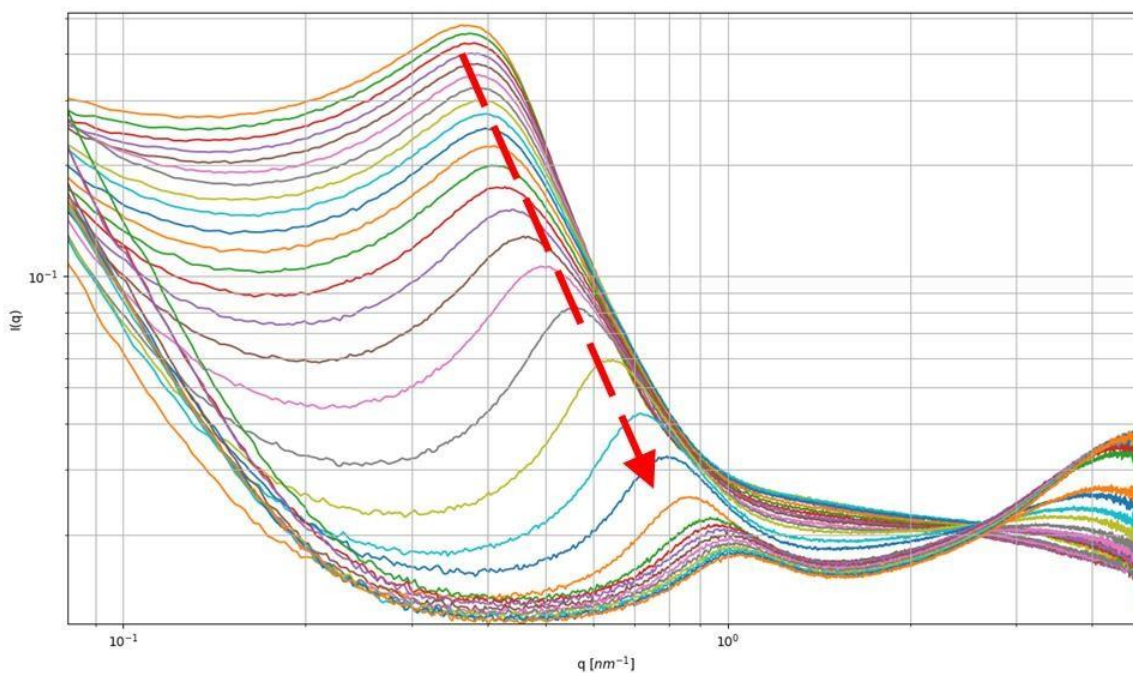

Figure 5.5: X-ray diffraction spectra of a swollen elastomer. The plot highlights the d_1 peak position, which corresponds to the spacing of backbones in the [41, 2] sample. The red dashed arrow highlights shift in the peak position of the d_1 peak. For this experiment, the sample was swollen in toluene for 24 hours and then let dry while measurements were collected every 2 min. The backbone spacing starts out at 17 nm and proceeds to decrease to 7 nm.

Here the red arrow shows the change in peak position, which reflects a subsequent decrease in the

d_1 spacing as solvent evaporates from the elastomer and the network strands move closer together.

In the fully swollen state, d_1 was found to be 17 nm, and decreased down to the dry state of 7 nm.

This is expected when compared to the swelling ratio that was measured for the [41,2,100] sample,

$Q_{eq} = 20.6$. If you assume that network expansion happens in an affine manner it would be

expected that the relative change in the spacing of the backbone should be equal similar $Q_{eq}{}^{1/3}$ and this is indeed the case for this situation.

 The spacing between backbones has been plotted against the composition parameter in **Figure 5.6**. The data shows two separate regimes of behavior for the samples that were measure. For the shortest sidechain length the spacing between strands increases by an exponent of -0.27 with respect to the composition parameter and for the longer sidechain lengths this exponent was found to be -0.55. This could be in part be due to some sort of segregation of the sidechains from the spacer during synthesis. In the case where of longer sidechains where the stearic hindrance is higher there is the chance that the actual grafting density would be slightly lower compared to a reaction with a shorter macromonomer. However, literature data suggests that the grafting density is should not vary significantly from the ratio of macromonomer to spacer present during synthesis.[3]
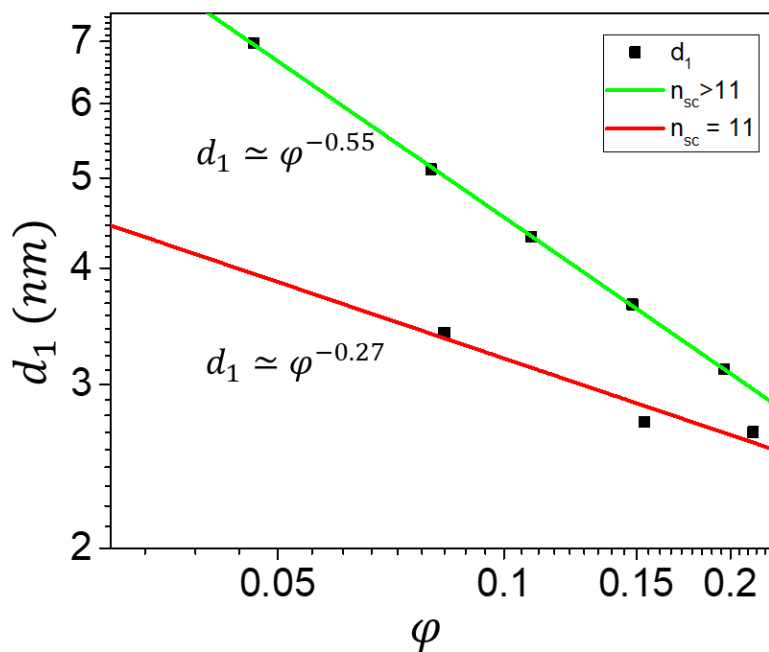
Figure 5.6: Backbone spacing correlation plot. The above graph shows the d_1 spacing plotted against the corresponding packing parameter, $\varphi = n_g/(n_{sc} + n_g)$. The data falls into two separate lines, the $n_{sc} = 11$ series (red) and the $n_{sc} = 23 \text{ and } 41$ series (green) each having a corresponding slope of -0.27 and -0.55.

REFERENCES

1. Keith, Andrew N., Charles Clair, Abdelaziz Lallam, Egor A. Bersenev, Dimitri A. Ivanov, Yuan Tian, Andrey V. Dobrynin, and Sergei S. Sheiko. "Independently Tuning Elastomer Softness and Firmness by Incorporating Side Chain Mixtures into Bottlebrush Network Strands." *Macromolecules* 53, no. 21 (2020): 9306-9312.

2. Rubinstein, Michael, and Ralph H. Colby. *Polymer physics*. Vol. 23. New York: Oxford university press, 2003.

3. Jacobs, Michael, Heyi Liang, Erfan Dashtimoghadam, Benjamin J. Morgan, Sergei S. Sheiko, and Andrey V. Dobrynin. "Nonlinear elasticity and swelling of comb and bottlebrush networks." *Macromolecules* 52, no. 14 (2019): 5095-5101.

CHAPTER VI

DIELECTRIC ELASTOMER ACTUATORS

6.1 Dielectric Elastomer Devices

Traditionally engineered machines are built from hard materials in rigid constructions that can efficiently execute a function in a controlled environment. Whereas biological machines found in nature are soft and adapt to their environment to execute a function under dynamic conditions. Traditional machines are not suited for applications that require the handling of soft materials as in surgery or navigating terrain under dynamic irregular conditions.[1]

Many actuating technologies are not useable for developing soft robots. Hydraulic actuators and electronic motors, although capable of producing large forces, are not suitable because their energy density is lowered by the use of heavy compressors or metal housings. They also have difficulty scaling down to smaller sizes. Piezoelectrics have a high energy density and can be scaled to meet a variety of different sizes, but the size of actuation strain produced is very small. This has led to the development of many new actuating concepts geared towards soft robotic applications. Electroactive polymers (EAPs) are one such category of materials; the most promising candidate being dielectric elastomers, whose performance is close to that of natural muscle in terms of actuation strain, pressure, and response speed.[2]
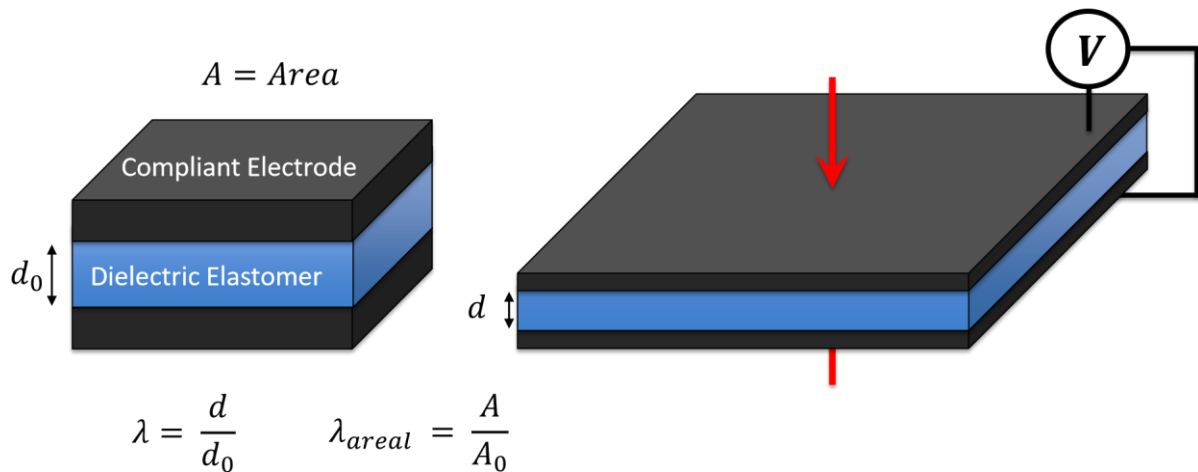
Figure 6.1: Dielectric elastomer device schematic. The schematic for a dielectric elastomer device is show in both the inactive (left) and active (right) state. The device moves from the inactive to the active state by the applied voltage V applied across the two flexible electrodes (black) on either side of the dielectric layer (blue). λ and λ_{areal} correspond to the stretching ratios for the dielectrics thickness and area for a given voltage and are used to characterize device performance.

Dielectric elastomers are a class of bio-inspired actuators that rapidly change shape when stimulated by an electric field. They are soft and continue to actuate even when an external mechanical strain is applied. Dielectric elastomers are also one of the leading technologies capable of matching the actuation properties of natural muscle.[3,4] Dielectric elastomer devices are composed of an elastic dielectric material sandwiched between two compliant electrodes. Application of a potential across the two electrodes results in a contraction of the material in the direction perpendicular to the electrodes and a concomitant expansion in the corresponding lateral directions (**Figure 6.1**).[3] Dielectric elastomers have been demonstrated to operate at large strains (>300% area strain), high response speeds (0.02-20 kHz), and relatively large actuation pressures (0.1-7 MPa).[5] However, their practical uses are limited by electromechanical instability, which is characterized by excessive thinning of the dielectric material at a critical voltage, which often leads to electrical breakdown.[6] To overcome this instability, the materials are pre-stretched with either a

rigid frame[3], interpenetrating polymer network[7], or swollen with a solvent[8]. Each method suppresses the electromechanical instability by stretching out the polymer material so that a nonlinear increase in stress is observed at smaller material deformations. However, each method also creates its own unique set of problems that further limit their use in dielectric elastomer devices. Rigid frames reduce device compliance and cause excessive wear on the dielectric material during operation. Interpenetrating polymer networks always result in an increase in modulus and complicate the fabrication process. Finally, solvents used to swell the dielectric material will always decrease the modulus, leak during actuation, and require encapsulation to prevent evaporation

6.2 Dielectric Elastomer Theory

Consider a dielectric elastomer device (**Figure 6.1**) to be a compliant capacitor, where the dielectric layer has a dielectric constant , initial thickness d_0, and initial area A_0. A voltage V is applied across the two compliant electrodes and the distance between them decreases to a length d. Also, at constant volume v, the area A_0 simultaneously expands to an area A. Unlike in a normal capacitor with capacitance $C_0 = {}_0 A_0/d_0$, the capacitance changes with respect to a stretching factor λ, where $\lambda = d/d_0$. This means for any λ, $C = \varepsilon \varepsilon_0 A/d = \varepsilon \varepsilon_0 V/(d_0^2 \lambda^2)$ is the capacitance relative to any thickness. The change in free energy of the system, ΔF, is given by the sum of electrostatic energy stored in the capacitor and the elastic energy stored in the dielectric layer as $\Delta F = \Delta F_{electric} + \Delta F_{elastic}$. For any elastomeric material under uniaxial deformation the change in free energy has already been investigated by Dobrynin *et al*[9], which gives the total change in free energy of the system as

$$\Delta F(V,\lambda) \cong -\frac{C_0 V^2}{2\lambda^2} + Gv\left[\frac{I_1(\lambda)}{6} + \beta^{-1}\left(1 - \frac{\beta I_1(\lambda)}{3}\right)^{-1}\right] \tag{6.1}$$

Where G is the shear modulus of the elastomer, $I_1(\lambda) = \lambda^2 + 2/\lambda$ is the first deformation invariant, and $\beta = R_0^2/R_{max}^2 = R_{max}b_k/R_{max2} \cong b_k/R_{max}$, where b_k is the Khun length, is a parameter that describes the elongation factor of an initial network strand in the elastomer material. The system approaches a stable equilibrium when the free energy is minimized – i.e., when

$$\frac{C_0 V^2}{\lambda^3} + \frac{Gv}{3}(\lambda - \lambda^{-2})\left[1 + 2\left(1 - \frac{\beta I_1(\lambda)}{3}\right)^{-2}\right] = 0 \tag{6.2}$$

This can be expressed as a function of the potential V applied across the two electrodes as

$$V = \lambda d_0 \sqrt{\frac{-\sigma_{true}(\lambda)}{\varepsilon\varepsilon_0}} \tag{6.3}$$

where $\sigma_{true}(\lambda)$ is the true stress in the material for any $\lambda < 1$, as seen in the literature.[9,10]

$$\sigma_{true}(\lambda) = \frac{G}{3}(\lambda^2 - \lambda^{-1})\left[1 + 2\left(1 - \frac{\beta(I_1(\lambda))}{3}\right)^{-2}\right] \tag{6.4}$$

6.3 Electric Breakdown

The maximum actuation strain and total force generated by a dielectric elastomer actuator is limited by the material's electrical breakdown strength. This makes it a very important property to understand in terms of both dielectrics in capacitors and in dielectric elastomers. The literature cites the general empirical relationship $E_B \propto d^{-n}$ for a wide range of materials (amorphous solids and crystalline ceramics), where E_b is the breakdown field strength, d is the thickness of the insulating dielectric, and n is a process dependent empirical constant for the specific material.[11]

Also, variance in breakdown strength in individual materials is usually observed because small imperfections such as voids, small inhomogeneities, mechanical vibrations, and sample contamination often lead to premature electrical breakdown in many materials. This means that the ultimate breakdown strength of a material can be well above the observed breakdown strength in a capacitor or dielectric elastomer (**Figure 6.2**).[12]
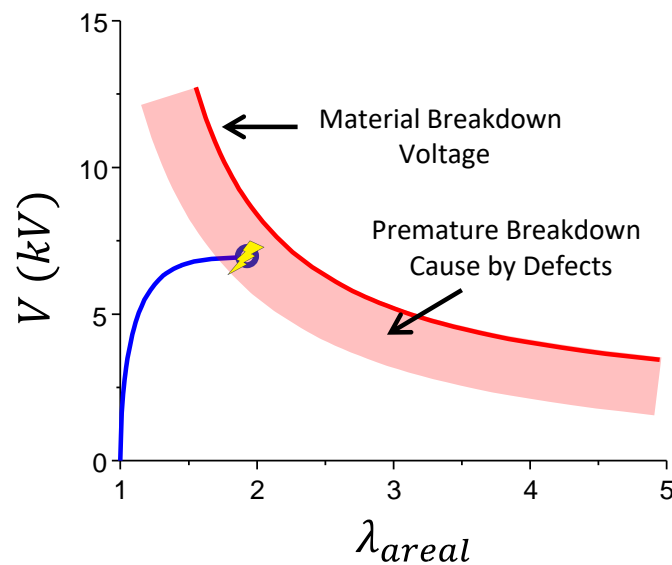

Figure 6.2: Electrical breakdown curve of a dielectric elastomer device. The figure shows the voltage strain curve of a dielectric elastomer device (blue) as it undergoes premature electrical breakdown due to a sample defect. The electrical breakdown curve (dark red) has a hard cutoff where the material will intrinsically breakdown at a given voltage and thickness of the material. However, defects in the material will almost always cause breakdown prior to this limit (light red).

In elastic polymer materials and dielectric elastomers, it is observed that the electrical breakdown strength of will increase with decreasing thickness and it will also increase if a biaxial pre-stretch is applied to the material.[11]

6.4 Electromechanical Instability

In dielectric elastomers, excessive thinning of the device followed by electrical breakdown at a constant voltage is referred to as an electromechanical instability. In **Figure 6.3**, three

theoretical materials were plotted using Eq. 6.3. The linear elastomer was calculated using $\sigma_{true} = G(\lambda^2 - \lambda^{-1})$ (**Figure 6.3A**), which is the solution to Eq. 2.3 for $\beta \approx 0$, goes through an electromechanical instability at the local maxima, $\lambda_{areal} = 1.59$ (**Figure 6.3B**).
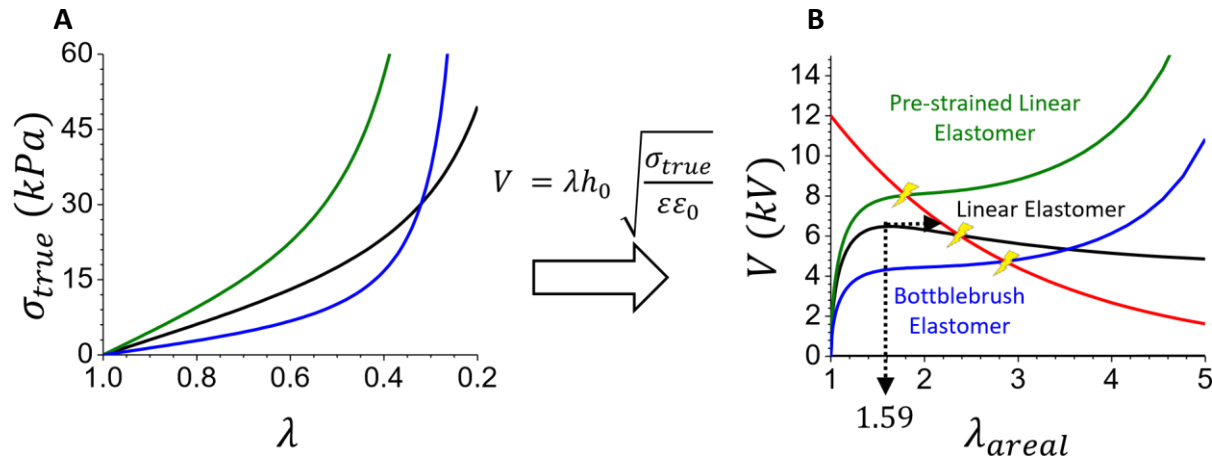

Figure 6.3: Stress strain curves ultimately dictate the magnitude and presence of an electromechanical instability. (**A**) Corresponds to the stress strain curves for a bottlebrush elastomer (blue), linear elastomer (black), and a pre-strained linear elastomer (green). These curves are transformed into voltage stress curves by equation Eq. 2.3. (**B**) Voltage stretch curves of the corresponding stress strain curves. The intersection of each material with the electrical breakdown curve (red) indicates where breakdown of the sample will occur. The pre-strained elastomer undergoes breakdown before significant actuation strain is achieved. The linear elastomer undergoes an electromechanical instability at $\lambda_{areal} = 1.59$ at which point it thins excessively to $\lambda_{areal} = 2.4$ and undergoes electrical breakdown. The bottlebrush elastomer achieves large actuation strains before breaking down and undergoes no instability.

Generally, linear elastomers around $\lambda_{areal} = 1.59$, at constant voltage, will immediately follow the dotted arrow and reach electrical breakdown because the network strands are usually highly coiled and flexible the force from the electric field pushing the two electrodes together becomes larger than the force of the material resisting deformation for any given small change in thickness. In linear elastomers, the approximation $\beta \approx 0$ is fairly accurate at small strains. The approximation

$\sigma_{true} = G(\lambda^2 - \lambda^{-1})$ fails to provide an accurate stress value at larger strains because it does not account for the nonlinear increase in stress observed when a network strand approaches its maximum extension. Instead, Eq. 6.4 must be used. This electromechanical instability severely hinders the actuation in dielectric elastomer devices, limiting many highly coiled and flexible linear elastomers to actuation below $\lambda_{areal} = 1.59$. Current materials are instead put under a biaxial pre-strain as mentioned above. After the linear elastomer undergoes biaxial pre-strain, there is no electromechanical instability. However, due to the materials increase in modulus, a larger potential in order to achieve actuation. Our lab has introduced a new materials design platform for dielectric elastomer devices based on bottlebrush network architectures. It can be seen in Figure 3 that the bottlebrush elastomer does not undergo an electromechanical instability and can still actuate at low applied electric fields.[10]

The reason linear elastomers undergo an electromechanical instability and bottlebrush elastomers do not is because the amount of pre-extension present in the bottlebrush elastomers network strands is high enough to cause a nonlinear increase in stress, which matches the nonlinear increase in force applied to the dielectric elastomer as its thickness decreases. This amount of preextension is characterized by the β parameter in Eq. 6.4. In linear elastomers, stress increases linearly with λ_{areal} and this results in an electromechanical instability because the force applied to the dielectric elastomer device increases the square of the distance between the electrodes.

6.5 PDMS Elastomer Synthesis

Polydimethylsiloxane elastomers were synthesized by mixing macromonomer monomethacryoxypropyl terminated polydimethysiloxane (MCR-M11, 12g, 12 mmol), methacryloxypropyl terminated polydimethyl siloxane (DMS-R18, 150-600 mg, 0.15-0.6 mmol),

anisole (9g), and phenylbis(2,4,6-trimethylbenzoyl)phosphine oxide (50 mg). The reaction mixture

was degassed with bubbling nitrogen for 30 minutes in the dark and injected into molds.

The molds were set under ambient light conditions for a minimum of 12 hours before removing
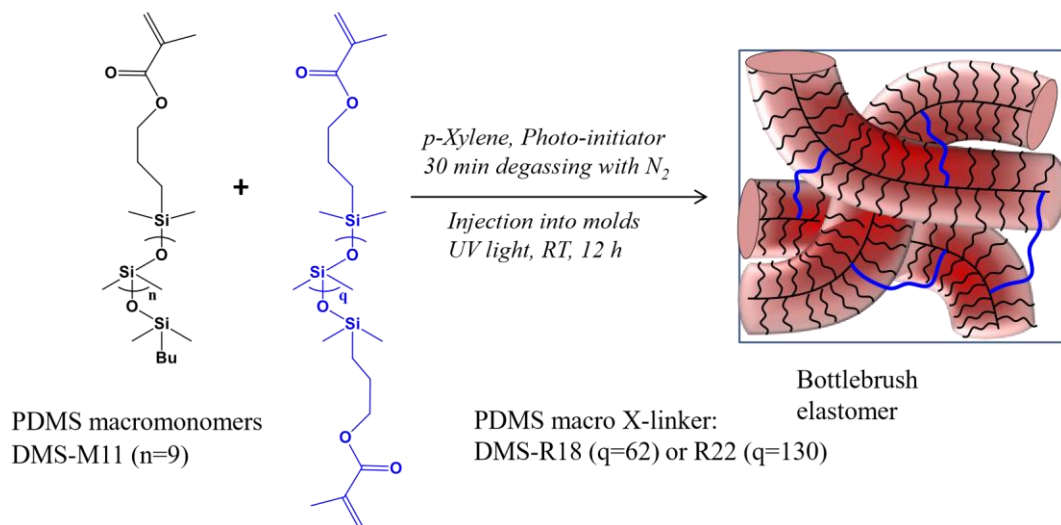
the elastomer (**Figure 6.4**).

Figure 6.4: Synthesis of PDMS bottlebrush elastomers. PDMS elastomers are synthesized in a
1 step polymerization of a PDMS macromonomer and a PDMS crosslinker that is ~5 times the
length of the macromonomer. The reaction is initiated by a photoinitiator and reaches its gel point
in ~30 min.

Gel fractions were measured by washing samples as mentioned above, exchanging the

solvent 5 times every 12 hours. For all crosslinking densities gel fractions above 90% were

obtained, which indicates that nearly all the monomers are being incorporated into the bottlebrush

network structure. Samples were tested to measure their dielectric constant, dynamic mechanical

analysis (DMA), and electrical actuation as a dielectric elastomer device under pre-strain free

conditions.

6.6 Electrical Actuation

To make sure that the electrical actuation experiments were performed under pre-strain free conditions, an in-house setup was created (**Figure 6.5**).
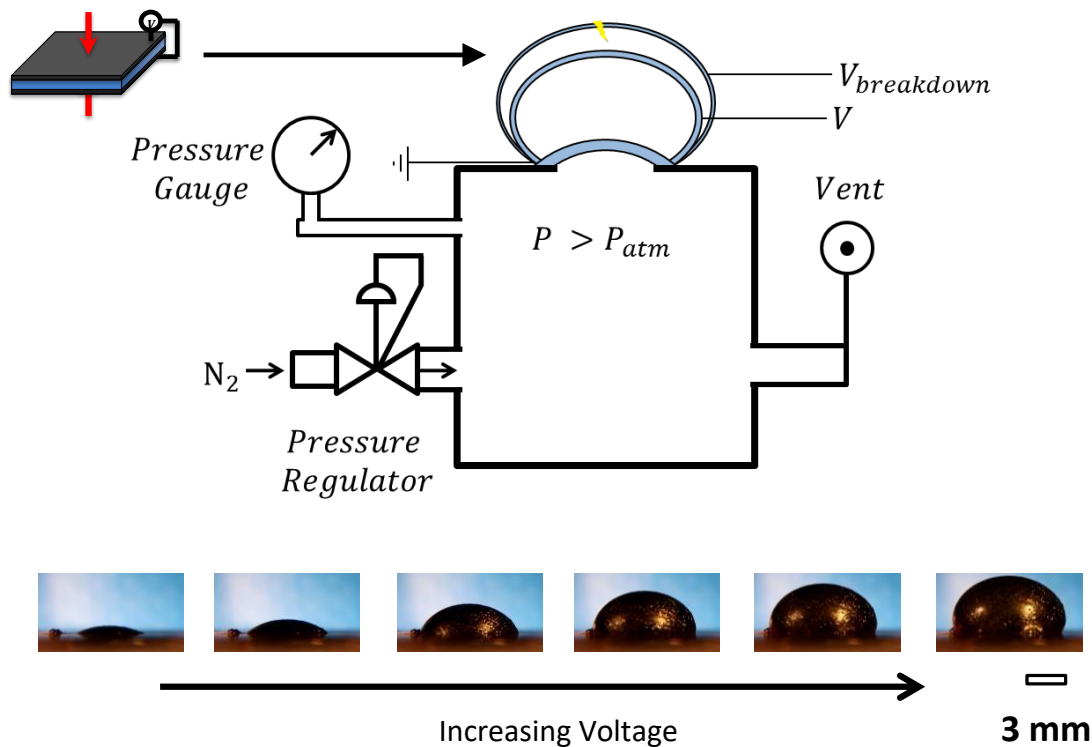

Figure 6.5: Diaphragm actuator schematic used for electromechanical characterization. The schematic shows that the dielectric elastomer device is attached to the top of a pressurized chamber where a slight bias pressure will cause the film to buckle upwards upon actuation. The bias pressure is kept constant throughout the entire experiment and is only slightly above atmospheric pressure so that it does not contribute to the perceived actuation strain. Below the schematic a series of images shows the actual strain produced by a dielectric elastomer device using this setup.

In this setup the dielectric elastomer device is placed on top of a small opening where a slight bias pressure is applied to one side, buckling the film upwards in a semi-sphere. As a voltage is applied to the device the dielectric covering the whole increases in area, causing the hemi-sphere

to increase in size until it finally reaches electrical breakdown. It is important to note that the bias pressure is small enough to ensure that the measured actuation strain is only caused by the application of an electric field. The actuation strain of the material was measured by calculating the surface area of the hemi-sphere from an image taken with a camera (**Figure 6.5**). When a dielectric elastomer device undergoes electromechanical instability characteristic wrinkling is seen in the film as sections of it stretch out unevenly when the sample undergoes the instability. This phenomenon has also been observed for these samples when they undergo an electromechanical instability.

In **Figure 6.6**, the results of electrical actuation experiments are shown alongside their theoretical predictions. It can be seen that theory and experiment match very well in the initial part of the experiment, but deviate towards the end. This is most likely due to the fact that the dielectric constant is assumed to be constant throughout the entire experiment. However, this is not the case in many materials and it is not taken into account in our model. In general, a decrease in the dielectric constant is normally seen in materials as strain increases. This happens because the network strands lose much of their freedom at higher strains, so they are not able to change their conformation and store as much energy from the electric field. The maximum actuation strain shown here is also on par with many pre-strained materials. This shows that bottlebrush elastomers are a promising new platform for materials design in dielectric elastomer devices.
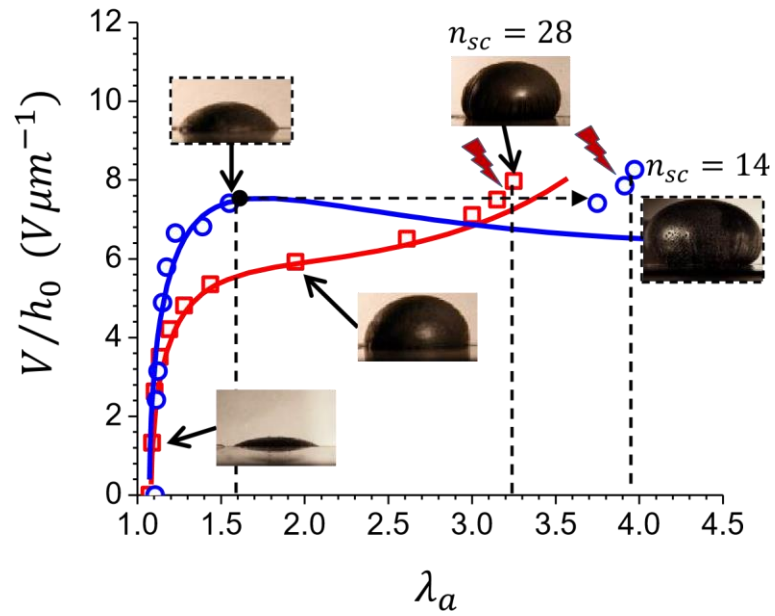
Figure 6.6: Electrical actuation of PDMS elastomers. The figure shows the electrical actuation of two PDMS bottlebrush elastomers. One elastomer undergoes an electromechanical instability (blue) and the other shows stable actuation until it reaches electrical breakdown (red). The theoretical model is shown as the solid lines and accurately represents the data in these experiments.

REFERENCES

1. Ilievski, Filip, Aaron D. Mazzeo, Robert F. Shepherd, Xin Chen, and George M. Whitesides. "Soft robotics for chemists." *Angewandte Chemie* 123, no. 8 (2011): 19301935.

2. Shankar, Ravi, Tushar K. Ghosh, and Richard J. Spontak. "Dielectric elastomers as nextgeneration polymeric actuators." *Soft Matter* 3, no. 9 (2007): 1116-1129.

3. Pelrine, Ron, Roy Kornbluh, Qibing Pei, and Jose Joseph. "High-speed electrically actuated elastomers with strain greater than 100%." *Science* 287, no. 5454 (2000): 836-839.

4. Carpi, Federico, Siegfried Bauer, and Danilo De Rossi. "Stretching dielectric elastomer performance." *Science* 330, no. 6012 (2010): 1759-1761.

5. Brochu, Paul, and Qibing Pei. "Dielectric elastomers for actuators and artificial muscles." In *Electroactivity in Polymeric Materials*, pp. 1-56. Springer, Boston, MA, 2012.

6. Suo, Zhigang. "Theory of dielectric elastomers." *Acta Mechanica Solida Sinica* 23, no. 6 (2010): 549-578.

7. Ha, Soon M., Wei Yuan, Qibing Pei, Ron Pelrine, and Scott Stanford. "Interpenetrating polymer networks for high-performance electroelastomer artificial muscles." *Advanced Materials* 18, no. 7 (2006): 887-891.

8. Vargantwar, Pruthesh H., A. Evren Özçam, Tushar K. Ghosh, and Richard J. Spontak. "Prestrain-Free Dielectric Elastomers Based on Acrylic Thermoplastic Elastomer Gels: A Morphological and (Electro) Mechanical Property Study." *Advanced Functional Materials* 22, no. 10 (2012): 2100-2113.

9. Dobrynin, Andrey V., and Jan-Michael Y. Carrillo. "Universality in nonlinear elasticity of biological and polymeric networks and gels." *Macromolecules* 44, no. 1 (2011): 140-146.

10. Vatankhah-Varnosfaderani, Mohammad, William FM Daniel, Matthew H. Everhart, Ashish A. Pandya, Heyi Liang, Krzysztof Matyjaszewski, Andrey V. Dobrynin, and Sergei S. Sheiko. "Mimicking biological stress–strain behaviour with synthetic elastomers." *Nature* 549, no. 7673 (2017): 497-501.

11. Huang, Jiangshui, Samuel Shian, Roger M. Diebold, Zhigang Suo, and David R. Clarke. "The thickness and stretch dependence of the electrical breakdown strength of an acrylic dielectric elastomer." *Applied Physics Letters* 101, no. 12 (2012): 122905.

12. Agarwal, V. K., and V. K. Srivastava. "Thickness dependence of breakdown field in thin films." *Thin solid films* 8, no. 5 (1971): 377-381.

13. Sheiko, Sergei S., Brent S. Sumerlin, and Krzysztof Matyjaszewski. "Cylindrical molecular brushes: Synthesis, characterization, and properties." *Progress in Polymer Science* 33, no. 7 (2008): 759-785.

14. Daniel, William FM, Joanna Burdyńska, Mohammad Vatankhah-Varnoosfaderani, Krzysztof Matyjaszewski, Jarosław Paturej, Michael Rubinstein, Andrey V. Dobrynin, and Sergei S. Sheiko. "Solvent-free, supersoft and superelastic bottlebrush melts and networks." *Nature materials* 15, no. 2 (2016): 183-189.

15. Zhang, Ling, Dongrui Wang, Penghao Hu, Jun-Wei Zha, Feng You, Sheng-Tao Li, and Zhi-Min Dang. "Highly improved electro-actuation of dielectric elastomers by molecular grafting of azobenzenes to silicon rubber." *Journal of Materials Chemistry C* 3, no. 19 (2015): 4883-4889.

16. Zhu, Zhenya, Alison G. Einset, Chia-Yu Yang, Wei-Xiao Chen, and Gary E. Wnek. "Synthesis of polysiloxanes bearing cyclic carbonate side chains. Dielectric properties and ionic conductivities of lithium triflate complexes." *Macromolecules* 27, no. 15 (1994): 4076-4079.

CHAPTER VII

SUMMARY & OVERALL OUTLOOK

8.1 Summary

In conclusion, this work this work has covered the synthesis of graft polymer elastomers and studied their mechanical properties in the dry state as well as when swollen in solvent. It was found that one distinct advantage of using a graft polymer architecture comes from the ability to decouple the structural modulus from its firmness parameter, which allows you to achieve many unique material properties that conventional elastomers cannot. In particular, for a series materials made from a network of linear polymers it is impossible to produce two materials that at the same solvent fraction have a different structural modulus. However, this can be accomplished using graft polymer architectures. Oscillatory shear rheology experiments on a series of comb like polymer melts was also able to show the architectural disentanglement that can be achieved by using graft polymers simply by changing their network architecture. It was also shown that graft polymer elastomers can be characterized independent of their link density by using cross-correlation between their structural modulus and firmness parameter. Specifically, these correlations changed depending on which specific regime (SSC, SBB, or comb) and through observing how G and β compare through a series of elastomers you better understand their behavior. Lastly, the electromechanical properties of PDMS dielectric elastomers were studied as they would apply to dielectric elastomers. It was found that they are particularly suited towards the development of devices that are capable of achieving high actuation strains at low applied voltages.

8.2 Future Work

Future work should focus on two parts the further development of acrylate elastomers towards applications where their specific mechanical properties necessary and the study of graft polymer elastomers as vibration dampening materials. Preliminary has been done on both parts and is included here. However, a more in depth study is needed to expand on these initial results.

First the PBA elastomers synthesized in chapter 3 are useful for studying basic properties of graft polymer elastomers because they are one singular composition. However, for them to be developed towards more useful applications it is important to expand the potential scope of functionalities that they can incorporate. One way this can be accomplished is by further functionalizing both ends of the oligomer sidechains to make functional macromonomers. This can be accomplished by synthesizing an ATRP initiator like 2-hydroxyethyl 2-bromoisobutyrate. By synthesizing oligomers with this particular initiator it is possible to synthesize macromonomers in high purity that also have an OH group on the chain end opposite that of the polymerizable methacrylate group. The OH functionality is particularly useful in this case because it can be used in many simple orthogonal click like reactions to make functional materials, but other synthetic routes could also be used.[1-5] The detailed synthesis that was used to make this specific initiator is below.

Materials. Ethylene glycol, α-bromosiobutyryl bromide, anhydrous sodium carbonate, anhydrous magnesium sulfate were received as purchased from Sigma Aldrich.

To a 250 mL round bottom flask equipped with a rubber septa 222 g of cold anhydrous ethylene glycol (3.6 mol) was stirred in an ice bath. 32.93 g α-bromosiobutyryl bromide (0.14 mol) was added dropwise over the course of 1 hour and left to stir overnight at room temperature.

The reaction mixture was added to 100 mL of deionized water and extracted into an organic phase by three sequential addition and extractions using 30 mL portions of DCM. The organic solution was then washed with water and saturated solution of sodium carbonate before drying voer anhydrous magnesium sulfate. Further separation was conducted by vacuum distillation at 60 C under reduced pressure. The extracted product was a clear viscous solution. The NMR spectrum of the product is included below (**Figure 7.1**).
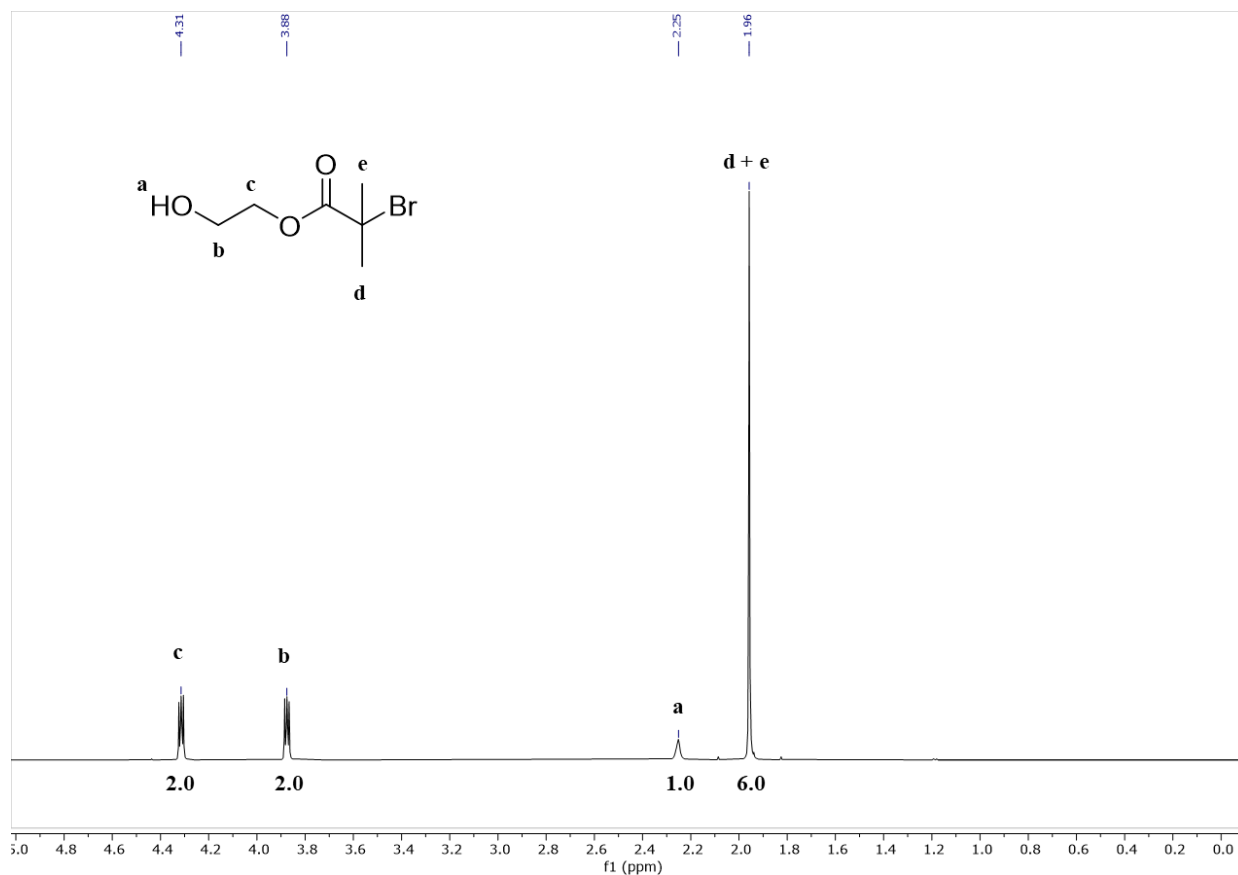

Figure 7.1: ^{1}H-NMR of functional initiator. (400 MHz, CDCl$_3$): 4.31 (HO-CH$_2$-**CH$_2$**-O-C=O, t, 2H), 3.88 (HO-**CH$_2$**-CH$_2$-O-C=O, t, 3H) 2.25 (**HO**-CH$_2$-CH$_2$, s, 1H), 1.96 (Br(CH$_3$)$_2$-C=O, s, 6H).

Bottlebrush elastomers are also particularly suited towards the development of vibration dampening materials.[6-8] This is largely due to the fact that their storage and loss modulus are

roughly equal over a broad range of frequencies. **Figure 7.2** shows the master curves that have been measured for plastomer materials that were studied previously.[9]
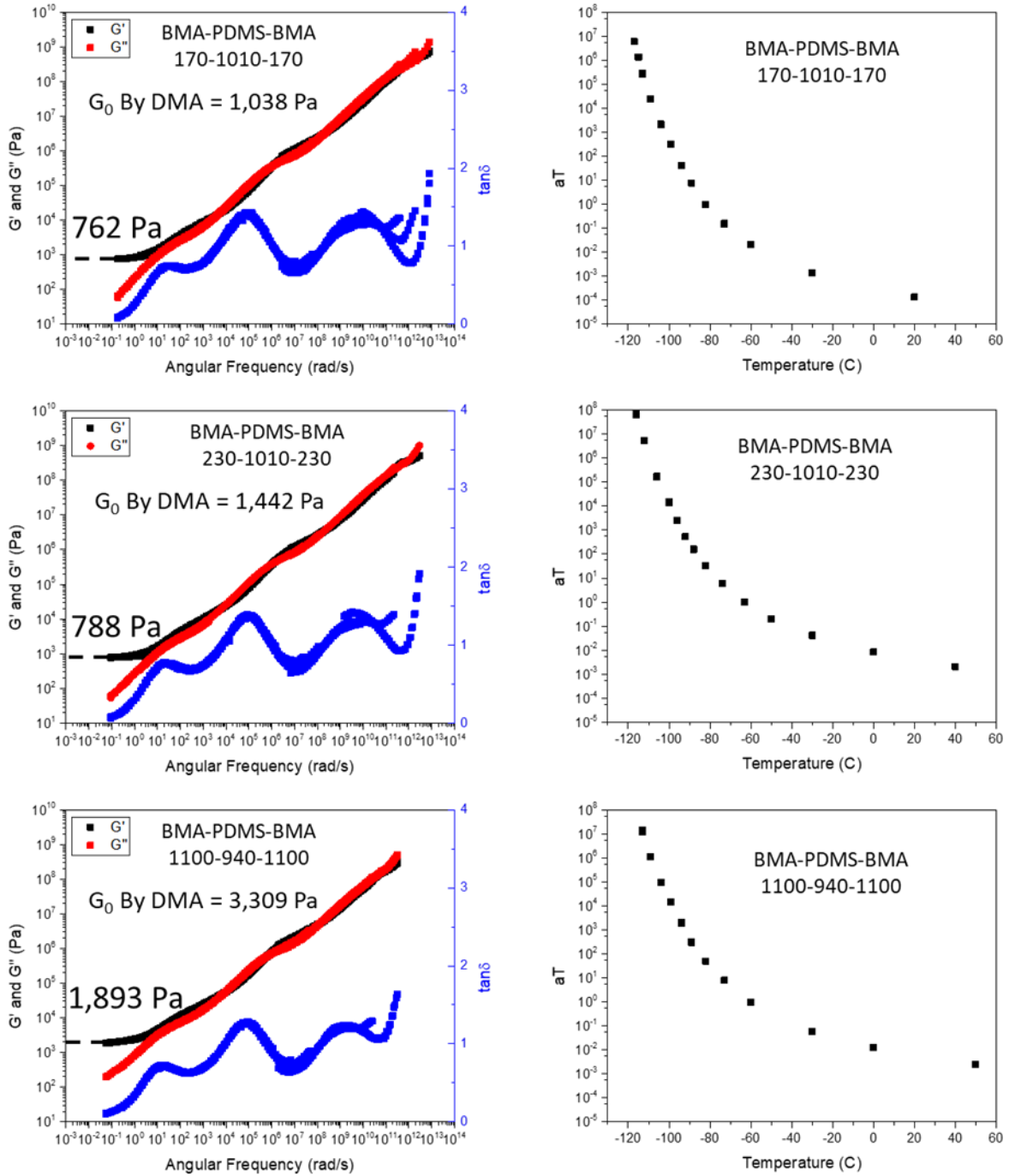

Figure 7.2: Rheological Master Curves a BMA-PDMS-BMA Plastomers. Dynamic Master curves (left) of the storage modulus G' (black points), loss modulus G" (red points), and $tan\delta$ (blue points) were measured for the graft polymers with (a) poly(butyl methacrylate) and (b)

poly(butyl acrylate) spacers between sidechains. Their corresponding WLF shift factors are shown to the left of each plot. Each plot was shifted from a reference temperature at -30 C, but frequencies are reported for 25 C.

The plastomers are synthesized by polymerizing PDMS macromonomers using a difunctional ATRP initiator. Then an ABA block copolymer is made by growing addition benzyl methacrylate linear segments on either side of the brush. Then when this polymer is dissolved in solvent and allowed to dry under ambient conditions it forms a physically crosslinked polymer network. For the measured samples it can be seen that the tan $\delta \sim 1$ for nearly all frequencies between the T_g and terminal relaxation plateau. This is the ideal material that one would want to use to passively damp mechanical waves. Since it works over such a broad range of frequencies these materials could even be applied towards acoustic and other high frequency applications.[10] Another noteworthy observation is the distinct shape of the tan δ curve for these elastomers. Three separate peaks are seen, which unique for an elastomeric material.[11] This phenomenon, although has been previously observed in the literature has not been particularly well studied and the underlying mechanism for this behavior is not known.

REFERENCES

1.   Tasdelen, Mehmet Atilla. "Diels–Alder "click" reactions: recent applications in polymer and material science." *Polymer Chemistry* 2, no. 10 (2011): 2133-2145.

2.   Golas, Patricia L., and Krzysztof Matyjaszewski. "Click chemistry and ATRP: a beneficial union for the preparation of functional materials." *QSAR & Combinatorial Science* 26, no. 11-12 (2007): 1116-1134.

3.   Lowe, Andrew B. "Thiol-ene "click" reactions and recent applications in polymer and materials synthesis." *Polymer Chemistry* 1, no. 1 (2010): 17-36.

4.   Kumar, Anuj, Rewati Raman Ujjwal, Apoorva Mittal, Archit Bansal, and Umaprasana Ojha. "Polyacryloyl hydrazide: an efficient, simple, and cost effective precursor to a range of functional materials through hydrazide based click reactions." *ACS Applied Materials & Interfaces* 6, no. 3 (2014): 1855-1865.

5.   Tsarevsky, Nicolay V., Brent S. Sumerlin, and Krzysztof Matyjaszewski. "Step-growth "click" coupling of telechelic polymers prepared by atom transfer radical polymerization." *Macromolecules* 38, no. 9 (2005): 3558-3561.

6.   Urayama, Kenji, Takashi Miki, Toshikazu Takigawa, and Shinzo Kohjiya. "Damping elastomer based on model irregular networks of end-linked poly(dimethylsiloxane)." *Chemistry of materials* 16, no. 1 (2004): 173-178.

7.   Chung, D. D. L. "Materials for vibration damping." *Journal of materials science* 36, no. 24 (2001): 5733-5737.

8.   Chung, D. D. L. "Structural composite materials tailored for damping." *Journal of Alloys and Compounds* 355, no. 1-2 (2003): 216-223.

9.   Vatankhah-Varnosfaderani, Mohammad, Andrew N. Keith, Yidan Cong, Heyi Liang, Martin Rosenthal, Michael Sztucki, Charles Clair et al. "Chameleon-like elastomers with molecularly encoded strain-adaptive stiffening and coloration." *Science* 359, no. 6383 (2018): 1509-1513.

10. Everhart, Matthew Hays. "Biologically Soft yet Ultrasonically Active Materials." PhD diss., The University of North Carolina at Chapel Hill, 2018.

11. Daniel, William FM, Joanna Burdyńska, Mohammad Vatankhah-Varnoosfaderani, Krzysztof Matyjaszewski, Jarosław Paturej, Michael Rubinstein, Andrey V. Dobrynin, and Sergei S. Sheiko. "Solvent-free, supersoft and superelastic bottlebrush melts and networks." *Nature materials* 15, no. 2 (2016): 183-189.